Science of the Total Environment 980 (2025) 179526

Contents lists available at ScienceDirect

Science of the Total Environment

journal homepage: www.elsevier.com/locate/scitotenv

Assessing modelled methane emissions over northern wetlands by the JULES-HIMMELI model

Yao Gao [a,b,*], Eleanor J. Burke [c], Sarah E. Chadburn [d], Maarit Raivonen [e], Tiina Markkanen [a], Mika Aurela [a], Lawrence B. Flanagan [f], Krzysztof Fortuniak [g], Elyn Humphreys [h], Annalea Lohila [a,e], Tingting Li [i], Ivan Mammarella [e], Olli Nevalainen [a], Mats B. Nilsson [j], Włodzimierz Pawlak [g], Aki Tsuruta [a], Huiyi Yang [k], Tuula Aalto [a]

[a] Finnish Meteorological Institute, P.O. Box 503, FI-00101 Helsinki, Finland
[b] Department of Civil Engineering, University of Hongkong, Hong Kong, China
[c] Met Office Hadley Centre, Exeter, UK
[d] Department of Mathematics, University of Exeter, Exeter, UK
[e] Institute for Atmospheric and Earth System Research (INAR)/Physics, Faculty of Science, University of Helsinki, P.O. Box 68, 00014 Helsinki, Finland
[f] Department of Biological Sciences, University of Lethbridge, 4401 University Drive, Lethbridge, Alberta, Canada
[g] Department of Meteorology and Climatology, Faculty of Geographical Sciences, University of Lodz, Lodz, Poland
[h] Department of Geography and Environmental Studies, Carleton University, Ottawa, Canada
[i] State Key Laboratory of Atmospheric Boundary Layer Physics and Atmospheric Chemistry, Institute of Atmospheric Physics, Chinese Academy of Sciences, Beijing 100029, China
[j] Department of Forest Ecology and Management, Swedish University of Agricultural Sciences, 901 83 Umeå, Sweden
[k] Livelihoods and Institutions Department, Natural Resources Institute, Faculty of Engineering & Science, University of Greenwich, UK

HIGHLIGHTS

- A process-based peatland CH_4 emission model was integrated with a land surface model.
- Optimized parameters improved the simulated CH_4 emission.
- Multi-site optimization performs better than the averages of single site optimization.
- Plant transport accounts for around 50 % of modelled CH_4 emissions.

GRAPHICAL ABSTRACT

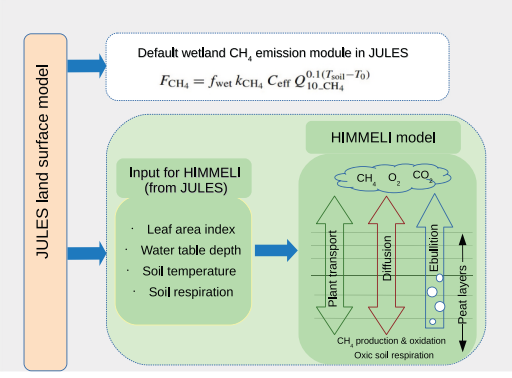

ARTICLE INFO

Editor: Kuishuang Feng

ABSTRACT

Northern wetlands are considered to be one of the most significant natural sources of methane (CH_4) emissions. The default wetland CH_4 emission scheme in JULES, a current state-of-art land surface model, only takes into account the CH_4 emissions from inundated wetland areas in a simple manner based on soil temperature and

* Corresponding author at: Finnish Meteorological Institute, P.O. Box 503, FI-00101 Helsinki, Finland.
E-mail address: yao.gao@hotmail.com (Y. Gao).

https://doi.org/10.1016/j.scitotenv.2025.179526
Received 13 September 2024; Received in revised form 31 March 2025; Accepted 22 April 2025
Available online 2 May 2025

Keywords:
Northern wetland
Methane emission
Modelling
Parameter optimization
Single-site optimization
Multi-site optimization

substrate availability. In this work, a process-based peatland CH_4 emission model HIMMELI was integrated with JULES, and the HIMMELI parameters were optimized with measured CH_4 flux at six northern wetland sites for each site separately or multi-sites simultaneously. The simulated CH_4 emission was significantly improved when using the optimized parameter values, with the bias of 54.88 mg m^{-2} d^{-1} averaged across all the studied sites in the simulation using the default parameter (DPR) values being reduced to −0.70 mg m^{-2} d^{-1} in the simulations using parameters values derived from the single site optimization (SSO) for each site. In the simulations using parameters values from the averages of single site optimization (SSO_AVG) and the multi-site optimization (MSO), the biases averaged across all the studied sites were −7.39 mg m^{-2} d^{-1} and −8.36 mg m^{-2} d^{-1}, respectively. The MSO simulations demonstrated more stable root mean square error (RMSE) between the simulated and observed methane emissions than the SSO_AVG simulations over the studied sites, when the RMSEs of SSO simulations were used as reference points. To further reduce the uncertainties in the simulated CH_4 emissions by the JULES-HIMMELI model, model processes related to the environment conditions (e.g. water table, soil carbon and vegetation) of wetland and northern wetland CH_4 emission processes (e.g. snow and ice covering effect) are suggested to be improved in JULES and HIMMELI, respectively. This study presents a comprehensive analysis of the impact of different parameters on the CH_4 emission in the JULES-HIMMELI model and obtains optimal parameter values for modelling CH_4 emissions at the studied northern wetlands. These findings pave the way for accurate regional estimates of northern wetland CH_4 emission.

1. Introduction

Methane (CH_4) is a powerful greenhouse gas with 28 times the global warming potential of carbon dioxide (CO_2) over a 100-year time scale (Myhre et al., 2013). Emissions and consequently atmospheric concentrations of CH_4 continue to increase, making CH_4 the second most important human-influenced greenhouse gas (GHG) after CO_2 (IPCC, 2021). Wetland CH_4 emission is not only the single largest but also the most uncertain natural source in the global CH_4 budget, accounting for around 24 % (158 vs. 664 Tg CH_4 yr^{-1}) to 29 % (166 vs. 575 Tg CH_4 yr^{-1}) of global CH_4 emissions estimated from bottom-up and top-down approaches between the year 2000–2020 (Saunois et al., 2024). Northern wetlands, located north of 30°N, take up to 50 % of the total global wetland area (Lehner and Döll, 2004). The wetland CH_4 emissions of northern wetland substantially contribute to the total terrestrial wetland CH_4 emissions by around 29 % (Saunois et al., 2024).

The relationships between wetland CH_4 emissions and its environmental controls are complex and remain unclear. In general, the controls on wetland CH_4 emission have been demonstrated to be soil temperature, water table depth (WTD) and vegetation. However, these relationships can be modified by wetland types, region and disturbance etc. (Rosentreter et al., 2021; Knox et al., 2019; Turetsky et al., 2014). Based on field measured CH_4 emissions, Yvon-Durocher et al. (2014) found a temperature dependence of seasonal variations in wetland CH_4 emissions, which is similar to the temperature dependence of CH_4 production derived from experiments based on pure cultures of methanogens and anaerobic microbial communities. Lupascu et al. (2012) illustrated that a lower water table stimulates lower CH_4 production potentials. However, H. Zhang et al. (2021) concluded that water level becomes less dominant for CH_4 production when sampling wetland sites with a wide range of nutrient gradients but similar water levels. Recently, Chen et al. (2021) showed that a lower WTD is associated with a decrease in the temperature dependence of CH_4 emissions and a higher WTD has the opposite effect, but WTD does not affect the temperature dependence of CO_2 emissions; i.e., wetland CH_4 emissions may be less sensitive to increasing temperature than CO_2 emissions when WTD is low, which could lead to changes in the ratio of CH_4 to CO_2 emissions and further climate impact (Huang et al., 2021). Vegetation provides the major source of organic matter in wetlands and plays an important role as one of the main pathways for methane transport to the atmosphere through their vascular tissues (Dorodnikov et al., 2011).

The strong sensitivity of wetland CH_4 emissions to environmental controls has raised concern on potential positive feedback under future climate change (Yuan et al., 2024; Zhang et al., 2023; Dlugokencky et al., 2009). Numerical models simulating wetland methane emissions with varied complexity have been developed for site- and regional-level and implemented in global climate and carbon cycle models, in order to quantify the magnitude, investigate the spatial and temporal variations, and understand the mechanism and environmental controls of wetland methane emission and its feedback to climate (Xu et al., 2016). Eight global-scale process-based models and two regional models with simple to relatively complex schemes in simulating wetland CH_4 emission were compared in the Wetland CH_4 Inter-comparison of Models Project (WETCHIMP) (Melton et al., 2013). Large divergences (about ±40 % of the all-model mean) were found in the modelled annual global wetland CH_4 emissions from the model ensemble in WETCHIMP. The large variations in simulated CH_4 emission rates were not only due to the uncertainties in wetland areas, but also the parameter and structural uncertainty in CH_4 emission models. Variable responses of methane emissions to temperature and precipitation in wetland-rich northern Europe in six land surface models have been found in Aalto et al. (2025). Nevertheless, modelling studies show that the potential positive feedback to climate change of wetland methane emissions can reduce the allowed anthropogenic emissions by around 8.0 % to maintain the Representative Concentration Pathways (RCP) 2.6temperature threshold (Gedney et al., 2019) and by up to 10 % to meet the Paris climate agreement (Comyn-Platt et al., 2018). Most northern wetlands are peatlands (Peltola et al., 2019). By integrating simulation results from five land surface models including peatland processes, northern peatlands are projected to be climate neutral under RCP2.6 but increase the global temperature by 0.21 °C under RCP8.5 by the year 2300 (Qiu et al., 2022).

The Joint UK Land Environment Simulator (JULES; Best et al., 2011; Clark et al., 2011) is the land surface scheme of the UK Earth System Model (UKESM) (Sellar et al., 2019), which contributed to the Coupled Model Intercomparison Project Phase 6 (CMIP6) model ensemble used by the most recent Intergovernmental Panel on Climate Change (IPCC) report (IPCC, 2021). JULES has also participated in multi-model comparison projects such as the Inter-Sectoral Model Intercomparison Project (ISIMIP; Rosenzweig et al., 2017) and the Global Carbon Project (GCP; Friedlingstein et al., 2022; Saunois et al., 2024). In addition, JULES has also been widely used to make global projections on hydrology, permafrost thaw, carbon and methane emissions (Burke et al., 2017; Chadburn et al., 2015a; Comyn-Platt et al., 2018; Gedney et al., 2019). Nevertheless, the default wetland CH_4 emission scheme in JULES is a simple function based on soil temperature and substrate availability, and the fraction of the saturated areas in a gridbox is used to calculated the grid box methane emissions. Chadburn et al. (2020) developed a microbial dynamic based wetland methane emission scheme for JULES and showed its capability in reproducing the observed seasonal dynamics of methane emissions in fully saturated wetland sites (Chadburn et al., 2020). However, as WTD is also an important factor controlling the wetland methane emissions (Chen et al., 2021; Huang et al., 2021), a wetland methane emission scheme considering the impact from

dynamics of WTD on wetland methane emissions is needed for JULES.

The HelsinkI Model of MEthane buiLd-up and emIssion for peatlands (HIMMELI; Raivonen et al., 2017) is a process-based peatland methane emission model. It can simulate CH_4 production and oxidation, as well as CH_4 transport by diffusion, ebullition and plant aerenchyma tissues in a layered peat column, which can contain water-filled and air-filled parts according to WTD. HIMMELI has been previously coupled with the other state-of-art land surface model, the Jena Scheme for Biosphere-Atmosphere Coupling in Hamburg (JSBACH), and the model framework has been applied in studying methane emissions from pristine peatlands and drained peatland forest (Li et al., 2024; Tyystjärvi et al., 2024; Kleinen et al., 2020).

In this study, we integrated HIMMELI with JULES, and evaluated the simulated CH_4 emissions by the JULES-HIMMELI model at six northern wetland sites. Model parameters of HIMMELI were optimized against measured CH_4 fluxes at each site individually and across multiple sites simultaneously, to explore the impact of parameter uncertainties while scaling up the JULES-HIMMELI simulations from site-level to regional-level. The main purpose of this work is to enhance the JULES model by incorporating a process-based peatland CH_4 emission model, and to assess its utility in simulating northern wetland CH_4 emissions with optimized model parameters, as well as to identify areas for future model improvements based on the discrepancies between modelled and observed CH_4 emissions.

2. Material and methods

2.1. Model description

2.1.1. Overview of JULES

JULES simulates physical, biophysical and biochemical processes that control the exchange of radiation, momentum, heat, water, carbon and nitrogen fluxes between the land surface and the atmosphere (Best et al., 2011; Clark et al., 2011; Harper et al., 2016; Wiltshire et al., 2021). JULES can be run as a standalone model driven with meteorological forcing data or as the land surface model of UKESM. The JULES version 5.8 release was used in this work.

JULES has a good representation of soil temperature and soil water, especially in cold regions (Chadburn et al., 2015a; Chadburn et al., 2015b; Chadburn et al., 2017), which are important environmental variables in simulating northern wetland methane emission. The default wetland methane emission scheme in JULES is a simple function based on soil temperature and substrate (which can be soil carbon, NPP or soil respiration) availability, and this is then multiplied by the fraction of inundated area in a gridbox to calculate the gridbox methane emissions (Gedney et al., 2004). The default wetland methane emission scheme in JULES has been updated to calculate the total wetland methane emission as the sum of methane production on multiple vertical soil layers (Comyn-Platt et al., 2018). Recently, a microbial dynamic based wetland methane emission scheme for JULES (referred as JULES-Microbe) has been developed and validated in fully saturated wetland sites (Chadburn et al., 2020). Equations of the multi-layer wetland methane emission scheme and JULES-Microbe can be found in Chadburn et al. (2020).

2.1.2. Overview of HIMMELI

HIMMELI simulates CH_4 build-up in and emission from peat soils (Raivonen et al., 2017). It describes microbial processes (including CH_4 production and oxidation, aerobic respiration) and three transport routes (diffusion in peat, plant transport, ebullition) in a layered one-dimensional peat column, keeping track of the concentration profiles of CH_4, O_2 and CO_2. The model is driven by the rate of anoxic soil respiration (anoxic Rs) for the area of the peatland, soil temperature profile along the soil column, LAI of aerenchymatous peatland vegetation, and WTD. It outputs CH_4, O_2 and CO_2 fluxes between the soil and the atmosphere, with the ability to separate the contributions of the three different transport routes. The model has been developed principally using a daily time step, but has also been tested on a 30-min time step and showed consistent output with the daily run. Previously, the model has been tested at two Finnish peatland sites (Siikaneva and Lompolojänkkä) and demonstrated its ability to simulate realistic CH_4 fluxes, when run with a combination of measured and simulated site-specific inputs (Raivonen et al., 2017). In this work, the HIMMELI v1.0 with a few bug corrections was adopted and was run with daily time resolution. The equations for methane production and oxidation, aerobic respiration, and methane transportation, as well as the bug corrections in HIMMELI are given in Appendix A. For more detailed description about the model please refer to Raivonen et al. (2017).

2.2. Site description

Six northern wetland sites located north of 45°N without substantial human influence on ecosystem functioning were selected for this study (Table 1). These sites are spread between the temperate and boreal climate zones. The wetland type includes both fen (five sites) and bog (one site), and the topography of these sites varies from relatively flat to hummock-lawn-hollow. Most of the sites are mainly covered by grass, sedge and mosses, but the two Canadian sites (i.e., Mer Bleue and Western Peatland) are dominated by shrubs or trees. The CH_4 fluxes were measured by eddy covariance (EC) towers at all the sites, with the timeseries length varying from 5 months to 96 months. Detailed descriptions of each site can be found in Appendix B.

2.3. Measurement data

2.3.1. Meteorological data and other site measurement data

CH_4 fluxes and meteorological data, as well as relevant ancillary data (such as WTD and soil temperature data) at the studied sites were mainly provided by the site principal investigators (PI). In order to prepare the meteorological diving data for the model simulations, the observed meteorological data for the studied sites (including shortwave and longwave radiation, air temperature, relative humidity, precipitation, air pressure, wind speed) were processed to 3-hourly temporal resolution, and then used to bias correct the long-term reanalysis Water and Global Change Forcing Data (WFD) from 1901 to 1979 and WATCH-Forcing-Data-ERA-INTERIM (WFDEI) data from 1979 to 2018 (Weedon et al., 2010; Weedon et al., 2014) from the gridboxes where the sites are located. Thus, the bias corrected meteorological forcing data covers the period from 1901 to 2018. The correction factors were generated by calculating monthly biases relative to the WFDEI data during the periods for which observed data were available. Those corrections were then applied to the whole period of the WFDEI data and the WFD data before 1979. More details of the bias correction method are described in Section 2.4 in Chadburn et al. (2017). The other in situ ancillary data including WTD, soil temperature were averaged to daily values to evaluate the simulation results from JULES.

Daily CH_4 fluxes at sites were needed for the comparison with the simulated CH_4 emissions. The observed CH_4 fluxes from site PIs for FI-SI (2005–2012) and CA-WP1 (2007) sites are at thirty-minute temporal resolution, and for FI-LO (2007–2018) and CA-MER (2011−2012) are at daily time resolution. The CH_4 flux for PL-KO (2013–2018) from site PIs is hourly gap-filled data. The thirty-minute CH_4 flux data were processed as described in Peltola et al. (2019) to derive the daily flux values, and the daily flux values for PL-KO were calculated as the daily averages of the gap-filled hourly data. Besides, observed CH_4 fluxes for the period from 2013 to 2018 for FI-SI and for the period from 2014 to 2018 for SE-DE with daily time resolution were obtained from the AVAA SmartSMEAR website (https://smear.avaa.csc.fi/download) and FLUXNET website (https://fluxnet.org/data/), respectively.

2.3.2. Sentinel-2 leaf area index (LAI) data

The daily Sentinel-2 LAI were obtained for 2017–2020 from the Sentinel-2 level-2A (L2A) products using the Google Earth Engine (GEE)

Table 1
Site characteristics of the studied wetland sites.

Sites (Abbre.)	Lat., Lon.	Climate zone	Wetland type	Peat depth (m)	Dominant vegetation	Climate (average temp. and precip.)	Data period and source, resolution	Reference
Siikaneva (FI-SI)	61.8 °N 24.2°E	Boreal	Oligotrophic (nutrient poor) Fen	2–4	Sedges, Rannoch-rush, peat mosses	3.3 °C and 713 mm	2005–2012, site PI, half-hourly; 2013–2018, SMEAR dataset, daily.	Aurela et al. (2007), Rinne et al. (2018)
Lompolojänkkä (FI-LO)	68.0°N 24.2°E	Boreal	Minerotrophic (mesotrophic (nutrient rich) Fen	2–3	Moss cover 57 %, sedges, birch, willow	−1.4 °C and 484 mm	2007–2018, site PI, daily.	Aurela et al. (2015, 2009)
Degerö Stormyr (SE-DE)	64.2 °N 19.6°E	Boreal	Minerogenic Oligotrophic (nutrient poor) Fen (a mixed acid mire)	3–4 m on average, up to 8 m	Sedges and mosses	1.2 °C and 523 mm	2014–2018, FLUXNET, daily.	Sagerfors et al. (2008)
Kopytkowo (PL-KO)	53.6°N 22.9°E	Temperate	Fen (mire)	2.5	Mixture of reeds, sedges, and rushes	6.6 °C and 583 mm	2013–2018, site PI, hourly.	Fortuniak et al. (2017, 2021)
Mer Bleue (CA-MER)	45.4°N −75.5°E	Temperate	Ombrotrophic bog	5–6 m at the center, 0.3 m at the margins	Dominant low status evergreen and deciduous shrubs, sparse cover of sedges and a few small trees, underlying moss	6.4+/− 0.8 °C and 943 mm	2011–2012, site PI, daily.	Lafleur et al. (2005), Moore et al. (2011), Brown et al. (2014)
Western Peatland 1 (CA-WP1)	55.0°N −112.5°E	Temperate	Moderately 'rich' treed Fen	~2	Dominated by stunted trees, with high abundance of a shrub, and a wide range of moss species.	2.1 °C and 504 mm	2007, site PI, half-hourly.	Long et al. (2010), Flanagan and Syed (2011)

and a Python implementation (Nevalainen, 2022) of the LAI algorithm in the Sentinel Application Platform (SNAP) software (Weiss and Baret, 2016). The data influenced by clouds and snow were filtered out according to the scene classification band available in the L2A product. The LAI values for each site were derived for a polygon with homogenized land cover around the site coordinate. The mean and standard deviation of the LAIs in the selected area were calculated to represent the site LAIs. The maximum LAI and its standard deviation of every year was selected from the time series, and then averaged over all the years to obtain the annual maximum LAI and its standard deviation for each site.

2.4. Simulation setup

The JULES simulation mainly followed the configuration in Chadburn et al. (2020) but with some modifications on the set up of plant functional type (PFT) as below. The model was set up with a 14-layered soil column reaching 3 m for both hydrothermal and carbon dynamics. The PFT was prescribed as 100 % C3 grass to represent the vegetation cover in pristine northern wetlands, as there is no vascular plants or mosses represented as JULES PFT. The maximum LAI for C3 grass was set to be 1.3 instead of 3, according to the site measured LAI in summer at Lompolojänkkä (Aurela et al., 2009). The meteorological forcing data were cycled over the years 1901–1920 to spin up JULES to equilibrium of soil hydrothermal and carbon quantities, and then the model was run until the end of 2018.

The soil and vegetation dynamics of a site (gridbox) simulated by JULES were used to drive HIMMELI when integrating HIMMELI with JULES. JULES simulates total soil respiration at distributed soil layers. The rate of anoxic Rs of the site, which is not directly simulated by JULES, was calculated as the average rate of total soil respiration in the soil below the simulated WTD. The simulated soil temperature profile along the prescribed soil layers in JULES was interpolated to match the soil layers in HIMMELI. To improve the accuracy of the JULES simulated WTD and LAI, those two variables were bias corrected according to the measured WTD and the annual maximum LAI derived from Sentinel-2 LAI data for the sites, respectively. The WTD was bias corrected by the delta change method, which means the JULES simulated WTD was corrected by adding the averaged bias between the simulated and observed WTD for a site. The JULES simulated daily LAIs were adjusted by multiplying the difference between them and the minimum LAI by a scaling factor and then adding the minimum LAI. The scaling factor was determined based on the ratio of the difference between annual maximum LAI derived from Sentinel-2 satellite data and the minimum LAI simulated by JULES to the differences between the maximum and minimum LAI simulated by JULES. For the two Canadian sites, CA-WP1 and CA-MER, the adjusted daily LAIs were further decreased to be 1/10 of their values, as the two sites are dominated by trees and shrubs, and the aerenchymatous vegetation acting as conduit for methane emissions is considered to take only a small proportion. Before adopting the JULES-HIMMELI model results, the HIMMELI model was spun up by repeating the driving data to reach an equilibrium of gas concentration profiles of CH_4, CO_2 and O_2.

2.5. Optimization of methane parameters

2.5.1. Optimized parameters

Ten parameters of the HIMMELI model were carefully selected to constrain the most important processes that contribute to the wetland CH_4 emission (Table 2). The lower and upper limits of these parameters were based on a combination of literature and expert knowledge. The physical meaning and the information regarding the parameter values is summarized in Table 2. f_m is the fraction controlling the methane production from anaerobic respiration of root exudates. $V_{R_{10}}$, $V_{O_{10}}$, ΔE_R, ΔE_{oxid} are oxidation and respiration parameters. $V_{R_{10}}$ is the respiration parameter controlling the rate of heterotrophic respiration, which consumes oxygen and thus affects oxygen availability for methane oxidation. $V_{O_{10}}$ is the CH_4 oxidation parameter controlling the potential rate of CH_4 oxidation. ΔE_R is a parameter affecting the temperature dependence of the heterotrophic respiration. ΔE_{oxid} affects temperature response of CH_4 oxidation. λ_{root}, a_{mA}, τ, $f_{D,a}$, $f_{D,w}$ are gas transport-related parameters. λ_{root} controls how the root mass is distributed. a_{mA} is the root-ending area per root biomass. τ is root tortuosity. A tortuosity of 1 means that the roots are not decreasing the conductance via their curvedness. $f_{D,a}$ is the fraction of the diffusion rate in air-filled peat divided by the diffusion rate in free air. Beside diffusion, $f_{D,a}$ also affects the plant transport rate (Eq. A15). $f_{D,w}$ is the same as $f_{D,a}$ but in water.

The parameters of HIMMELI that were not optimized are listed in Table 3. The three Michaelis-Menten constants for aerobic respiration

Table 2
List of parameters driving the production, oxidation and transport scheme in HIMMELI that have been optimized.

Parameters	Definition	Unit	Ranges	Default value	References
f_m	Fraction of anaerobic respiration becoming methane	–	[0, 0.8]	0.5	Raivonen et al. (2017)
$V_{O_{10}}$	Potential CH_4 oxidation rate at 10 °C	mol m^{-3} s^{-1}	[$2e^{-6}$, $3e^{-4}$]	1e-5	Raivonen et al. (2017); Segers (1998).
$V_{R_{10}}$	Potential rate of aerobic peat respiration at 10 °C	mol m^{-3} s^{-1}	[$2e^{-6}$, $1e^{-4}$]	1e-5	Nedwell and Watson (1995); Watson et al. (1997)
λ_{root}	Decay length (in root distribution)	m	[0.01, 0.4]	0.2517	Wania et al. (2010)
a_{mA}	Root ending area per root dry biomass	m^2kg^{-1}	[0.05, 0.4]	0.085	Stephen et al. (1998)
τ	Root tortuosity	–	[1.0, 5.0]	1.5	Stephen et al. (1998)
$f_{D,a}$	Reduction factor for diffusion in air-filled peat	–	[0.01, 1]	0.8	Raivonen et al. (2017)
$f_{D,w}$	Reduction factor for diffusion in water-filled peat	–	[0.01, 1]	0.8	Raivonen et al. (2017)
ΔE_R	Active energy of aerobic respiration	J mol^{-1}	[$2e^4$, $8e^4$]	50,000	Nedwell and Watson (1995)
ΔE_{oxid}	Active energy of oxidation	J mol^{-1}	[$2e^4$, $8e^4$]	50,000	Nedwell and Watson (1995)

Table 3
List of parameters that were not optimized.

Parameters	Definition	Unit	Default value	References
K_R	Michaelis-Menten constant for aerobic respiration reaction	mol m^{-3}	0.02	Nedwell and Watson (1995)
K_{o_2}	Michaelis-Menten constant for O_2 in oxidation	mol m^{-3}	0.03	Nedwell and Watson (1995)
K_{CH_4}	Michaelis-Menten constant for CH_4 in oxidation	mol m^{-3}	0.03	Raivonen et al. (2017)
k	time constant for ebullition	s^{-1}	1/1800	Raivonen et al. (2017)
SLA	specific leaf area of gas-transporting plants	m^2 kg^{-1}	15	Raivonen et al. (2017)
η	sensitivity of methanogenesis to oxygen	m^3 mol^{-1}	400	Arah and Stephen (1998)
σ	peat porosity	–	0.85	Raivonen et al. (2017)

reaction (K_R), O_2 oxidation (K_{o_2}), and CH_4 in oxidation (K_{CH_4}) were considered to need large amounts of data to constrain (Susiluoto et al., 2018). The time constant for ebullition (k) was determined by the temporal resolution of the observed data. The specific leaf area (SLA) of gas-transporting plants was not optimized as a_{mA} and τ for the calculation of plant transport rate of gas X in Eq. (A15) were both optimized. η describes the sensitivity of methanogenesis to oxygen, which is a microbial activity related parameter. It was dropped from optimization because f_m in Eq. (A4), the factor controlling the fraction of anaerobic respiration becoming CH_4, was optimized. The peat porosity σ was left out for optimization as diffusivity parameters $f_{D,a}$ and $f_{D,w}$ were optimized.

2.5.2. Optimization method

The parameter optimization process was conducted using the Shuffled Complex Evolution – University of Arizona (SCE-UA; Duan et al., 1994) algorithm implemented in the Statistical Parameter Optimization Tool for Python (SPOTPY; Houska et al., 2015). The SCE-UA algorithm is a global optimization method that efficiently explores the parameter space to find the optimal parameter set. SPOTPY provides a user-friendly interface for implementing the SCE-UA algorithm and facilitates the calibration of complex models with a large number of parameters. The root mean squared error (RMSE) between the observed and simulated methane emissions was chosen as the objective function. The RMSE is a commonly used metric in model calibration and represents the average difference between the observed and simulated values, taking into account both the magnitude and direction of the differences. By minimizing the RMSE, the model parameters can be adjusted to improve the agreement between the observed and simulated methane emissions, ultimately enhancing the model's predictive accuracy. In the optimization run, iterative simulations were performed until a global minimum was reached, ensuring that the solution was not limited to a local minimum.

Two types of optimization runs were conducted over the site-specific observation period in this study. The single site optimization (SSO) for which parameters were optimized for each site individually and the multi-site optimization (MSO) that aimed at refining one set of parameters considering multiple sites together. For the SSO of Siikaneva (FI-SI), Lompolojankka (FI-LO), Degero (SE-DE) and Kopytkowo (PL-KO), a leave-one-year-out cross validation (LOO-CV; see, e.g. Gelman et al., 2013) method was performed. This was done to obtain the mean and uncertainties of the optimized parameters from multiple optimization runs with different input data series. The SSO runs for the Mer Bleue (CA-MER) and West Peatland 1 (CA-WP1) sites were performed for the entire observation period due to the limited data length. The optimized parameter values from the SSO at the six study sites were then averaged to acquire the averages of single site optimization (SSO_AVG) parameter values, in order to compare with the parameter values optimized from the MSO. For the MSO, ten years of data from the following sites were prepared to give equal weight to each site in the optimization run: FI-SI (selected data period: 2007–2016) and FI-LO (selected data period: 2008–2017), SE-DE (selected data period: 2014–2018in combine with 2014–2018) and PL-KO (selected data period: 2013–2017 in combine with 2014–2018). The two Canadian sites, CA-WP1 and CA-MER, were excluded from the MSO runs due to too short data period in comparison to the other sites. In the MSO runs, one year of data from each site was left out sequentially in each optimization run to obtain the mean and uncertainties from a group of optimized parameter values. Therefore, there were a total of ten MSO runs, with nine years of data from each site in each MSO run.

3. Results

3.1. Simulated environmental variables

3.1.1. Water table depth

Overall, the simulated WTD is lower than the observed WTD at FI-SI, FI-LO, PL-KO and SE-DE sites, but is slightly overestimated at CA-MER and CA-WP1 sites (Fig. 1). For the simulated WTD at FI-SI, the timing

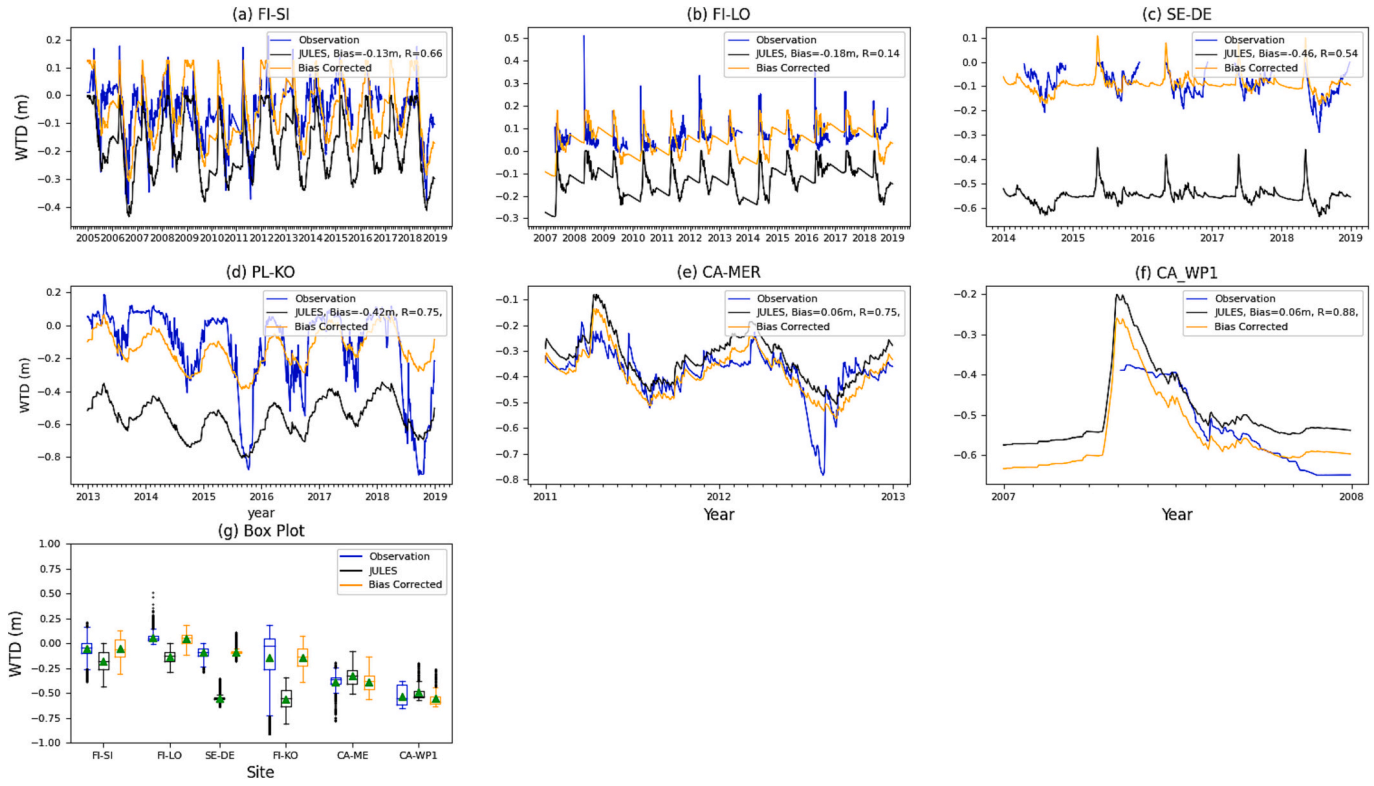

Fig. 1. Observed, simulated and bias corrected daily water table depth (WTD) at each site. The box plot shows the median (line), mean value (green triangle), Q1 (25%) and Q3 (75%) quartiles of the data (the bottom and top of the box), and the lower and upper whiskers represent the range of 1.5 times interquartile range (Q3-Q1) from the Q1 and Q3. The data points outside the 1.5 times interquartile range can be considered as extremes. The same period as the observed methane flux was selected for the WTD data, and the statistics shown in the figure were calculated by filtering the simulated WTD according to the availability of observed WTD.

of water table drawdown from the saturated soil (above zero WTD) in spring is mostly well captured, but the WTD in summer for most years over the study period is underestimated. Moreover, the water table draw up in the second half of year is much delayed. This simulated drying of the soil is because excess water becomes surface runoff from the top soil layer or subsurface runoff from the bottom layer when the soil column is saturated in JULES, instead of ponding. The bias corrected WTD at FI-SI reduces the underestimation of WTD especially in summer and the

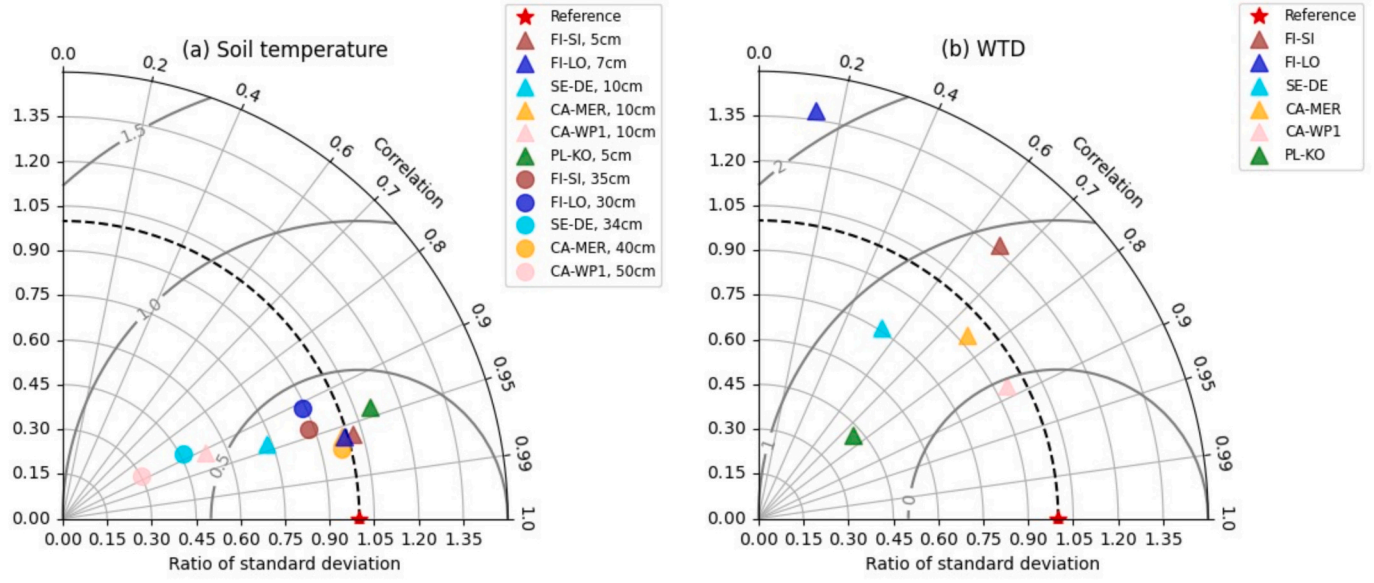

Fig. 2. Taylor diagrams of soil temperature at (a) shallow (5–10 cm; shown in triangles) and deeper (34–50 cm; shown in circles) soil depths; (b) water table depth (WTD). All statistics were calculated using daily averaged data over the available observational period. All points were normalized by dividing the standard deviation of model results by the standard deviation of the corresponding measurements; thus, the reference point of ratio of standard deviation is 1.0. Sites are represented with different colors. For the Kopytkowo site, the soil temperature is only measured at 5 cm. (The time series of observed and simulated soil temperatures are shown in Fig. S1 in the supplementary).

second half of year. FI-LO is a site with above surface WTD most of the time. However, as the default JULES hydrology scheme is not able to simulate continuously saturated soil or store extra stagnant water above the surface, and there are no lateral flow inputs to the soil column, the WTD in JULES drops when the temperature increases and becomes saturated in a short period due to snow melt. The dynamics of WTD at FI-LO is not well described in JULES, with the lowest correlation coefficient ($R = 0.14$) in all the studied sites. Nevertheless, the bias corrected WTD is above surface most of the time over the studied 12 years, which is similar to the observed WTD. Also, the timing of the spring peaks of the observed WTD over the years are well captured by the model. The wetland CH_4 emissions simulated in HIMMELI are not as sensitive to the changes in the thickness of water layer above the peat surface as to the changes in WTD below the surface in the processes of CH_4 oxidation and transportation. Thus, it is more proper to use the bias corrected WTD to simulate CH_4 emissions in FI-LO by HIMMELI. The bias between the observed and simulated WTD at SE-DE is the biggest (−0.46) in the studied sites, but the fluctuation of WTD is generally well described ($R = 0.54$) and the ratio of standard deviation of the simulated to observed WTD is 0.76 (Fig. 2 (b)). The ratio of standard deviation demonstrates the difference in the standard deviations between the simulated and observed soil temperatures, where the reference point is 1.0. The dynamics of the observed WTD at PL-KO and CA-MER are well simulated by JULES ($R = 0.75$) at both sites. However, the bias at the PL-KO site (bias = −0.42 m) is much larger than the bias at the CA-MER site (bias = 0.06 m). Also, the ratio of standard deviation of the simulated to observed WTD in PL-KO (0.42) is the smallest in the sites. This is because the JULES simulated WTD is damped and does not show the extreme low water table events (WTD < −0.8 m) in 2015 and 2018. The very dry summer of 2012 at CA-MER is not captured by JULES. The simulated and observed WTD at CA-WP1 showed highest correlation coefficient in the sites ($R = 0.88$) and small bias (0.06 m) over the period from May to December of 2007 with observed WTD.

3.1.2. Soil temperature

To compare the simulated and observed soil temperatures at the same depth, the simulated vertical soil temperature profile in JULES was linearly interpolated to the depth of observed soil temperature. The time series of soil temperature at the studied sites can be seen in Fig. S1 in supplementary. The simulated soil temperatures at both shallow (5–10 cm) and deeper (34–50 cm) soil depth show strong correlation ($R \geq 0.88$) with the observed soil temperatures at all the sites (Fig. 2 (a)). Except for SE-DE and CA-WP1, the ratio of standard deviation of the simulated to observed soil temperature for other sites is close to the reference point with values between 0.88 and 1.10. Both shallow and deeper soil temperatures at the SE-DE site were underestimated throughout the year in the period with observed data. The maximum difference of the daily soil temperature between model and observations at SE-DE reached 9.3 °C of the deeper soil layer in the summer of 2014. For CA-WP1, the soil temperature at the shallow soil layer is overestimated in winter and underestimated in summer in JULES, while the soil temperature in the deeper soil layer is underestimated in summer but close in the winter and spring months in 2007. The soil temperature at the shallow and deeper soil layers of CA-MER are slightly underestimated overall in JULES. For sites (FI-SI, FI-LO and PL-KO) with above surface water table and above zero soil temperature in winter according to the observation, the JULES simulated soil temperature at shallow soil depth is underestimated with below zero temperature as the simulated WTD is below surface and the soil at shallow layers was unsaturated (Fig. 1). On the contrary, JULES simulated soil temperature at the surface soil layer in summer is overestimated at those three sites due to the unsaturated soil at the surface. However, JULES simulated soil temperature at the deeper soil layers are underestimated slightly at FI-SI and FI-LO sites.

3.1.3. Leaf area index (LAI)

Compared to the annual maximum LAI values derived from Sentinel-2 satellite data, the prescribed maximum LAI in our JULES simulation is lower for most of the sites except for SE-DE (Fig. 3(a)). The JULES simulated LAI is updated daily by multiplying the maximum LAI by a scaling factor, which is calculated with temperature-dependent leaf turnover rates (Clark et al., 2011). From Fig. 3 (b) we can see that the JULES simulated LAIs at those six sites have the same maximum value but different seasonal cycles. The PL-KO is the site with the earliest increase of LAI in spring and the FI-LO is the latest one. JULES simulates unrealistic high LAI in wintertime, but we did not correct the simulated LAI in winter due to the lack of measured LAI in winter. The bias corrected LAIs at sites show large differences in the maximum LAI according to the maximum LAIs derived from Sentinel-2 data. PL-KO has the largest LAI values compared to other sites. The bias corrected LAIs for CA-WP1 and CA-MER are very small with the maximum value of 0.179. This is because those two sites are dominated by trees and shrubs (Table 1) and 1/10 of the bias corrected LAI according to the maximum LAIs derived from Sentinel-2 data was assumed to be the LAI of aerenchymatous plants acting as conduits for methane emissions in this study.

3.2. Optimized parameters

The results of the optimized parameter values are presented in Table 4. In comparison to the default value of f_m, the optimized values of f_m were significantly decreased from 0.5 to a range from 0.063 to 0.257. $V_{O_{10}}$ increased for most of the investigated sites in the SSO and in the MSO, but it decreased for SE-DE and CA-WP1. ΔE_{oxid} only decreased in the SSO for the two Canadian sites. $V_{R_{10}}$ increased for most of the sites except for CA-WP1 in the SSO and in the MSO. ΔE_R decreased in the SSO for all sites as well as in the MSO. The uncertainties of $V_{O_{10}}$ at FI-SI, FI-LO, SE-DE and MSO are quite large. On the contrary to $V_{O_{10}}$, the uncertainties of $V_{R_{10}}$ at FI-LO, SE-DE and MSO are small. λ_{root} is smaller for most sites in the SSO and MSO runs than the default value, except for PL-KO. λ_{root} in the MSO is also increased. Nevertheless, the uncertainties of λ_{root} at PL-KO and MSO are much smaller than the other sites. a_{mA} increased in all the SSO and MSO runs. In general, $f_{D,a}$ and $f_{D,w}$ decreased, while τ increased after optimization, except in the SSO simulations of CA-WP1 and CA-MER. The uncertainties of $f_{D,a}$ and $f_{D,w}$ at PL-LO are the largest in all the sites. Overall, the uncertainty of $V_{O_{10}}$ is the largest in all the parameters.

3.3. Simulated methane emissions

The observed and simulated time series of CH_4 emissions in the simulations using parameter values from DPR, SSO, SSO_AVG and MSO (referred as the DPR simulation, SSO simulation, SSO_AVG simulation and MSO simulation below) for the studied sites are shown in Fig. 4. At all the sites, the summertime CH_4 emissions in SSO, SSO_AVG and MSO simulations are largely decreased compared to the CH_4 emissions in the DPR simulation. The CH_4 emissions in the SSO_AVG simulation closely follow the CH_4 emissions in the SSO simulations at FI-SI, SE-DE and PL-KO sites. However, the CH_4 emissions in the SSO_AVG simulation are too low at FI-LO and CA-WP1, and too high at CA-MER compared to the observed and simulated CH_4 emissions in the SSO simulations. To understand the effects of optimized model parameters on CH_4 emissions simulated by the model, the CH_4 emissions in the SSO and MSO simulations were mainly compared below.

FI-SI, FI-LO and SE-DE are boreal fen sites which emit > 40 mg m^{-2} d^{-1} CH_4 from the observations averaged over the study period. FI-LO locates the northernmost and the CH_4 emission is highest in the studied sites. The total CH_4 emission and the CH_4 emission through the three transport pathways at FI-SI in the SSO simulation and MSO simulation are comparable (Table 5). However, the total CH_4 emission of the SSO simulation for FI-LO is approximately double than that of the MSO

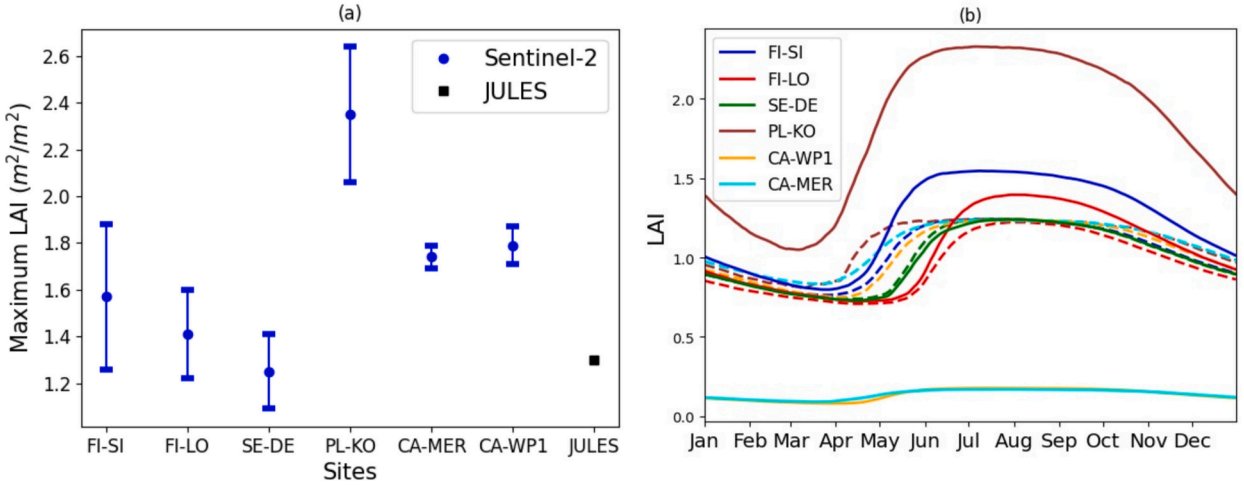

Fig. 3. a) Maximum leaf area index (LAI) and its standard deviation over the selected area from Sentinel-2 satellite data for each site, and the maximum LAI value that was set in the JULES simulations; b) Seasonal cycle of JULES simulated LAI (dashed lines) and bias corrected LAI according to the maximum LAI from Sentinel-2 data (solid lines). The bias corrected LAIs for CA-WP1 and CA-MER was then decreased to be 1/10 of their values to represent the LAI of aerenchymatous plants acting as conduits for methane emissions at those sites according to the site characteristics.

Table 4
Parameter values from the single site optimization (SSO), averages of single site optimization (SSO-AVG) and multi-site optimization (MSO) for each site. Uncertainties for the optimized parameters are in the parentheses.

	f_m	$V_{O_{10}}$ (mol m^{-3} s^{-1})	$V_{R_{10}}$ (mol m^{-3} s^{-1})	λ_{root} (m)	a_{mA} ($m^2 kg^{-1}$)	τ	$f_{D,a}$	$f_{D,w}$	ΔE_R (J mol^{-1})	ΔE_{oxid} (J mol^{-1})
FI-SI	0.10	2.66e^{-5}	8.08e^{-5}	0.182	0.253	2.911	0.519	0.429	31,716.53	62,247.07
	(0.04)	(3.17e^{-5})	(2.45e^{-5})	(0.065)	(0.084)	(1.382)	(0.241)	(0.229)	(9788.27)	(11,898.25)
FI-LO	0.20	1.16e^{-5}	8.75e^{-5}	0.198	0.251	3.06	0.593	0.472	28,086.12	63,030.02
	(0.13)	(1.58e^{-5})	(9.04e^{-6})	(0.055)	(0.083)	(1.267)	(0.270)	(0.301)	(9387.91)	(15,314.29)
SE-DE	0.13	8.18e^{-6}	8.73e^{-5}	0.113	0.284	2.457	0.667	0.432	23,535.74	69,692.62
	(0.09)	(1.08e^{-5})	(5.39e^{-6})	(0.029)	(0.065)	(0.658)	(0.201)	(0.213)	(5932.47)	(14,217.62)
PL-KO	0.063	6.01e^{-5}	7.17e^{-5}	0.378	0.108	3.584	0.258	0.438	30,243.13	60,390.15
	(0.016)	(2.55e^{-5})	(2.41e^{-5})	(0.032)	(0.045)	(0.912)	(0.316)	(0.385)	(14,840.93)	(18,476.97)
CA-WP1	0.257	2.07e^{-6}	7.02e^{-6}	0.100	0.384	1.007	0.978	0.668	44,621.4	38,332.3
CA-MER	0.106	3.76e^{-5}	5.74e^{-5}	0.175	0.306	1.032	0.409	0.997	20,279.2	21,573.7
SSO_AVG	0.143	2.44e^{-5}	6.53e^{-5}	0.191	0.265	2.342	0.571	0.573	29,747.02	52,544.31
MSO	0.095	4.27e^{-5}	7.64e^{-5}	0.349	0.198	2.627	0.297	0.552	36,398.58	66,166.03
	(0.04)	(3.25e^{-5})	(1.03e^{-5})	(0.043)	(0.080)	(0.878)	(0.192)	(0.201)	(8572.88)	(13,804.08)

simulation, which is in line with the higher value of f_m in the SSO compared to the MSO (Table 4). The differences in total CH_4 emission at FI-LO are mainly presented in the CH_4 emission through plant transport, while the amount of CH_4 emitted through diffusion and ebullition are similar in the SSO and MSO simulations (Table 5). The higher CH_4 emission through plant transport in the SSO simulation may be attributed to the higher a_{mA}, which leads to increased root conductance, although the lower λ_{root} and higher τ in the SSO simulation can counteract the effect of higher a_{mA}. In the simulations for the SE-DE site, the total CH_4 emission in the SSO and MSO simulations are close. However, the CH_4 emission through plant transport in the SSO simulation (11.57 g m^{-2} yr^{-1}) is nearly two times higher than that in the MSO simulation (6.30 g m^{-2} yr^{-1}) due to the higher a_{mA} and lower τ in the SSO.

PL-KO is a representative of temperate Central and Eastern European wetlands (Fortuniak et al., 2021). It showed very high methane emission in the first two years of measurements, i.e. June of 2013 and July of 2014, but much lower emission in the following years. However, the high CH_4 emission in 2013 and 2014 are not captured by the simulations. Nevertheless, the lower CH_4 emission in 2015 compared to other years was captured by the model. The peaks of CH_4 emission in 2016, 2017 and 2018 happened in May in the observation, which is earlier than other years, when WTD was still relatively high, but temperature had risen enough for an intensive methanogenesis. Moreover, the higher f_m and lower $V_{O_{10}}$, but similar $V_{R_{10}}$ in the MSO compared to those in the SSO, lead to a higher total methane emission in the MSO simulation than in the SSO simulation at PL-KO. The CH_4 emission through plant transportation in the MSO simulation (6.85 g m^{-2} yr^{-1}) is approximately twice as large as in the SSO simulation (3.52 g m^{-2} yr^{-1}) due to the higher a_{mA} and lower root tortuosity in the MSO, both of which increase root conductance. The differences in $f_{D,a}$ and $f_{D,w}$ between the SSO and MSO are too small to significantly affect CH_4 emission through diffusion.

CA-WP1 is a tree dominant temperate fen with limited observation data. At CA-WP1, from the end of April till the mid of May in 2007, there is a strong increase in the production of CH_4 and also a small increase in the oxidation of CH_4 in the simulations. A sharp increase of WTD due to snowmelt and a warming up of soil temperature to be above zero happened in this period. The strong increase of CH_4 production leads to around 20 mg m^{-2} d^{-1} CH_4 accumulated in the soil in the beginning of this period and released mainly through plant transport in May and then through diffusion with dropping down of the WTD. In the CA-WP1 simulations, the total CH_4 emission in the SSO simulation is about four times higher than that of the MSO simulation, and the f_m is two times higher in the SSO of CA-WP1 compared to the MSO. Additionally, the nearly two times lower $V_{O_{10}}$ but similar $V_{R_{10}}$ in the SSO simulation, leads to more CH_4 emission due to the lower oxidation rate of CH_4. The higher CH_4 emission in the SSO simulation compared to the MSO simulation at CA-WP1 is mainly shown in diffusion, which is 6.24 g m^{-2} yr^{-1} in the SSO simulation but 0.82 g m^{-2} yr^{-1} in the MSO simulation.

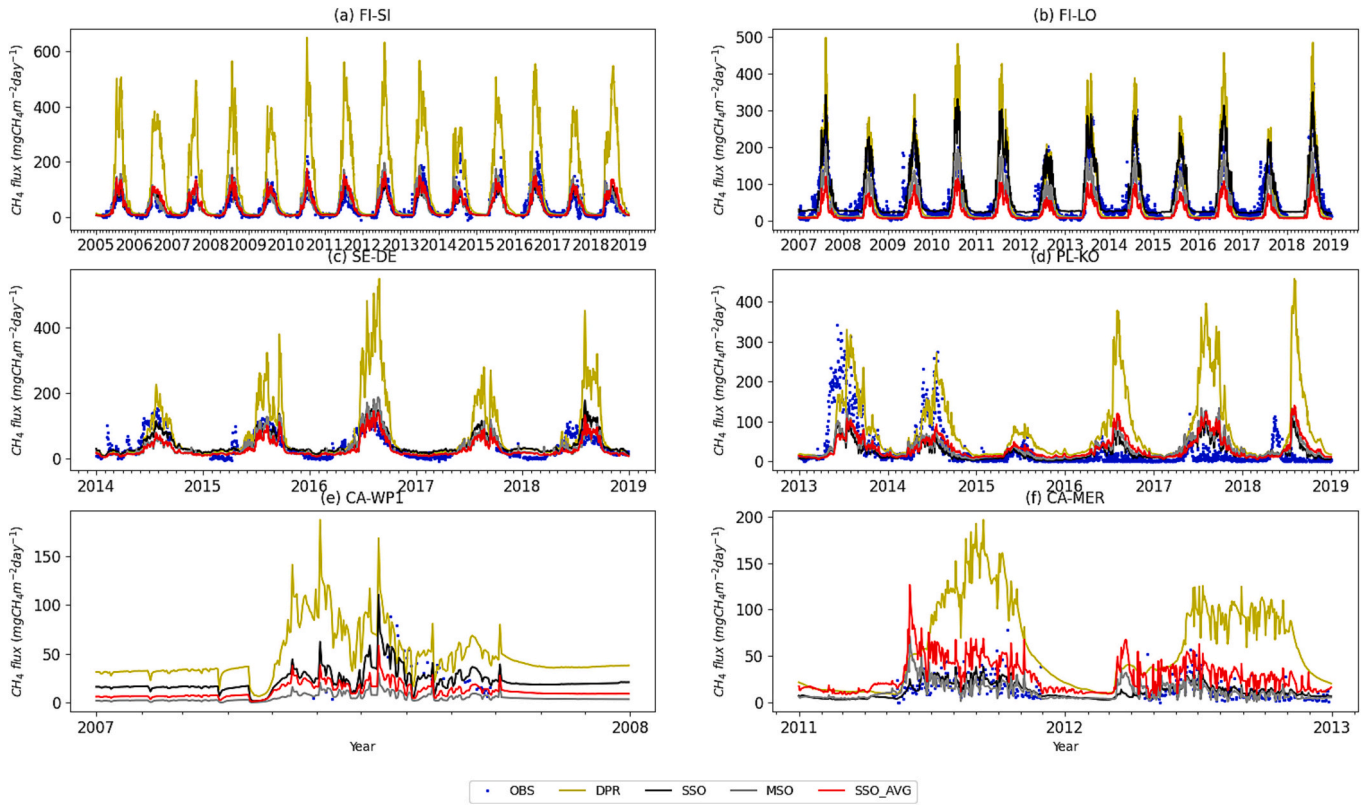

Fig. 4. Observed (blue dots) and simulated methane emissions from simulations using default parameter values (DPR; green line), and simulations using parameter values from single site optimization (SSO; black line), averages of single site optimization (SSO_AVG; red line) and multi-site optimization (MSO; gray line).

Table 5
Yearly averaged methane (CH_4) emissions, production, oxidation and CH_4 emitted by diffusion, plant transport, and ebullition from simulations employing optimized parameters obtained from the single site optimization (SSO) and multi-site optimization (MSO).

Site	Simulation	CH_4 emission (g m^{-2} yr^{-1})	CH_4 production (g m^{-2} yr^{-1})	CH_4 oxidation (g m^{-2} yr^{-1})	Diffusion (g m^{-2} yr^{-1})	Plant transportation (g m^{-2} yr^{-1})	Ebullition (g m^{-2} yr^{-1})
FI-SI	SSO	12.85	26.01	13.19	5.19	7.43	0.24
	MSO	14.98	32.95	17.98	7.53	6.93	0.51
FI-LO	SSO	24.77	35.02	10.27	1.69	17.5	5.58
	MSO	11.80	26.48	14.69	1.34	5.71	4.75
SE-DE	SSO	16.31	20.61	4.39	4.71	11.57	0.03
	MSO	12.58	26.13	13.64	6.20	6.30	0.08
PL-KO	SSO	9.09	22.18	13.14	5.26	3.52	0.32
	MSO	11.68	29.53	17.89	4.64	6.85	0.19
CA-WP1	SSO	8.04	10.24	1.83	6.24	1.8	0
	MSO	1.88	4.75	2.7	0.82	1.06	0
CA-MER	SSO	4.06	10.52	6.48	1.60	2.46	0
	MSO	4.19	9.72	5.55	2.44	1.75	0

This can be attributed to the larger $f_{D,a}$ and $f_{D,w}$ in the SSO compared to the MSO at CA-WP1.

CA-MER is the only bog site in this study. It is located the south most and its vegetation cover is shrub dominated. The CH_4 emission at CA-MER from observation is the smallest in the sites with < 20 mg m^{-2} d^{-1} on average. For the CH_4 emission at CA-MER, the total CH_4 emission in the MSO simulation is only slightly higher than in the SSO simulation. The root conductance in the SSO simulation is higher than that in the MSO simulation due to higher a_{mA} and lower τ, and this leads to higher CH_4 emission through plant transportation in the SSO simulation than in the MSO simulation. $f_{D,a}$ and $f_{D,w}$ in the SSO simulation are both higher than in the MSO simulation, however CH_4 emission through diffusion is lower in the SSO simulation than in the MSO simulation.

In general, plant transport dominates the CH_4 emission in winter in the SSO simulation, except for CA-WP1 (Fig. 5). In summer, diffusion dominates the CH_4 emission in the SSO simulation except for FI-LO and SE-DE, where plant transport takes the biggest fraction of the total CH_4 emission. The simulated CH_4 emission in winter at CA-WP1 is dominated by diffusion due to the highest diffusion rates and smallest λ_{root} compared to other sites, as well as the very low WTD reaching around −0.6 m. In the year 2006, 2009, and 2018 of FI-SI, 2015 of PL-KO, which showed lower bias corrected WTD compared to other years at the sites, the simulated CH_4 production and emission are smaller than other years. The model simulations with the optimized parameters performed well in those dry years (Fig. 4).

In the MSO simulation, diffusion dominates the summertime CH_4 emission and plant transport dominates the wintertime CH_4 emission at all the studied sites (Fig. 6). Ebullition to the surface is a small fraction of the total emission, from 0 to 3.5 % in our studied sites except FI-LO. The ebullition to the atmosphere at FI-LO is the highest in the studied sites, which takes 23 % and 40 % of total CH_4 emission in the SSO and MSO simulations (Fig. 7). There is no ebullition to the surface at CA-WP1 and

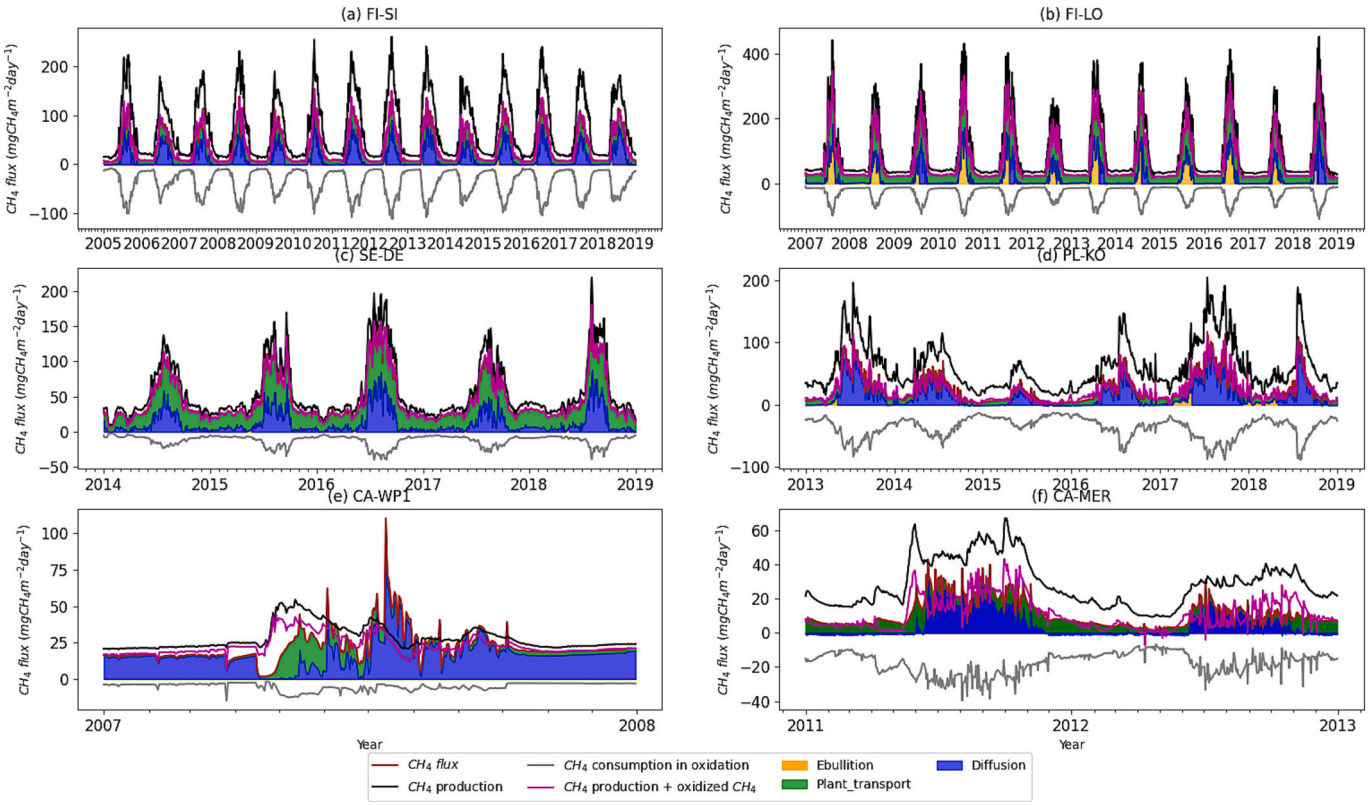

Fig. 5. Methane production and oxidation, CH4 consumption in oxidation, as well as methane emissions through diffusion, plant transport, and ebullition in the simulations using parameter values derived from single site optimization (SSO).

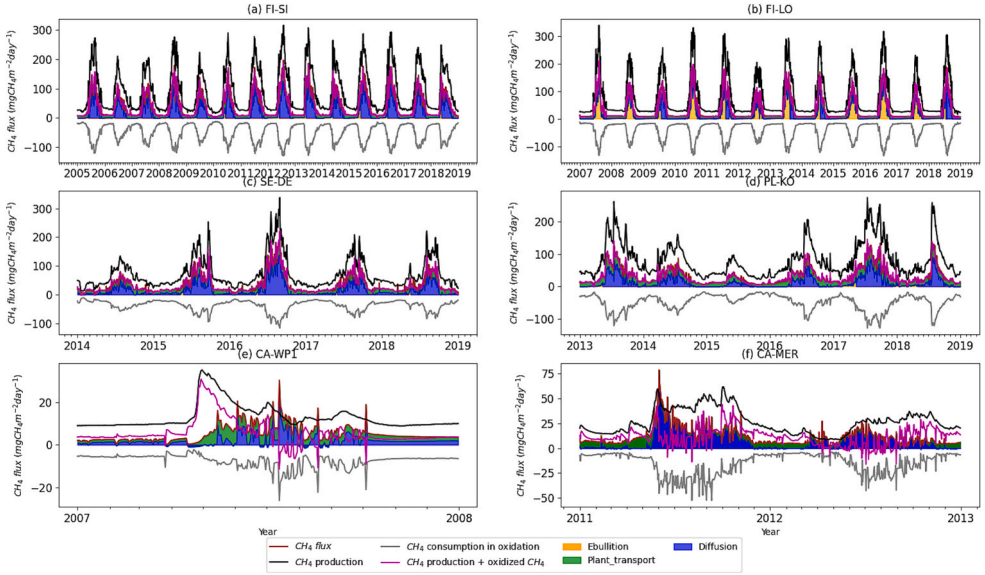

Fig. 6. Simulated methane production and oxidation, as well as methane emissions through diffusion, plant transport, and ebullition in multi-site optimization (MSO).

CA-MER in both the SSO and MSO simulations as HIMMELI only produces ebullition to the surface when WTD is above ground.

The inter-annual variability of the oxidized CH_4 in the rhizosphere is closely related to the dynamics of CH_4 production (Fig. 5 & Fig. 6). The proportion of the oxidized CH_4 in the produced CH_4 emission at FI-LO, SE-DE and CA-WP1 are 29 %, 21 % and 18 % in the SSO simulation, respectively. Those numbers are much lower than the fraction of oxidized CH_4 in the rhizosphere at other sites and at the MSO simulations, which are over 50 %. This is mainly because the lower $V_{O_{10}}$ at the FI-LO, SE-DE and CA-WP1 than the other sites in the SSO (Table 4).

3.4. Comparison between the simulated and observed methane emissions

The simulated and observed CH_4 emissions were compared through a set of statistical metrics. For all the studied sites, the mean of the

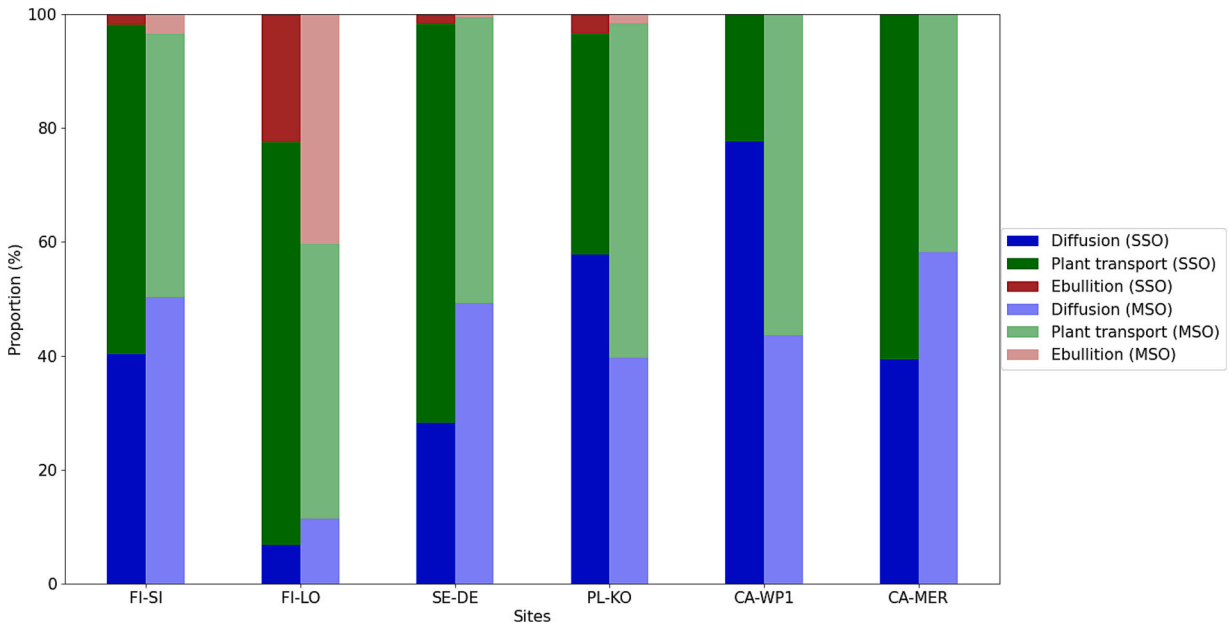

Fig. 7. Proportions of the amount of methane transported through diffusion, plant transport and ebullition to the total methane emission in the single site optimization (SSO) and multi-site optimization (MSO).

simulated CH_4 emissions of the DPR simulation is higher (54.88 mg m^{-2} d^{-1} (20.03 g m^{-2} yr^{-1}) on average) than the mean of the observed CH_4 emissions at all the studied sites, with the minimum bias of 0.48 mg m^{-2} d^{-1} at FI-LO and the largest bias at CA-MER of 121.56 mg m^{-2} d^{-1} (Table 6). Those positive biases of the CH_4 emissions in the DPR simulations are largely reduced in the SSO, SSO_AVG and MSO simulations, except for the FI-LO. The overestimation averaged over all the sites is reduced to −0.7 mg m^{-2} d^{-1} (−0.26 g m^{-2} yr^{-1}) in the SSO simulation, while the simulated CH_4 emission averaged over all the sites were underestimated by −7.39 mg m^{-2} d^{-1} (−2.70 g m^{-2} yr^{-1}) and −8.35 mg m^{-2} d^{-1} (−3.05 g m^{-2} yr^{-1}) in the SSO_AVG simulation and the MSO simulation, respectively. The mean bias of FI-LO increased from 0.48 mg m^{-2} d^{-1} in the DPR simulation to 8.65 mg m^{-2} d^{-1} in the SSO simulation, and −38.98 mg m^{-2} d^{-1} and -27.12 mg m^{-2} d^{-1} in the SSO_AVG and MSO simulations, respectively. In the DPR simulation of FI-LO, the overestimation of CH_4 emission in summer is compensated with the underestimation of CH_4 emission in winter and in the shoulder period. However, in the SSO simulation of FI-LO, the overestimation of CH_4 emission in summer is largely decreased to fit better with the observed emission but the CH_4 emission in wintertime turns to be overestimated. The negative biases of the SSO_AVG and MSO simulations of FI-LO are due to the underestimation of CH_4 compared to observed CH_4 all through the year. Nevertheless, the correlation coefficient increase in the SSO, SSO_AVG and MSO simulations of FI-LO and the RMSE decrease in the SSO and MSO simulations compared to the DPR simulation at this site (Table 7). The correlation coefficient between the observed and simulated CH_4 emissions from the SSO simulation are highest compared to other simulations for all the studied sites (Table 6 & Fig. 8). The correlation coefficient between the observed and the simulated CH_4 emissions from the SSO_AVG simulation are improved in all the sites compared to the DPR simulation. However, the correlation coefficient between the observed and the simulated CH_4 emission from the MSO simulation is decreased in the FI-SI, CA-MER sites compared to the DPR simulation. The ratios of standard deviation of the simulated to observed CH_4 emission are also improved (i.e., decreased from too big values in the DPR simulation to smaller values in the optimized simulations) at all the studied sites, except for CA-WP1 (Fig. 8). Nevertheless, the centered RMSE shown with the gray contours of CA-WP1 decreases in the optimized simulations compared to the DPR simulation. In general, the centered RMSE of the optimized simulations decreases compared to the DPR simulation for all the studied sites, except for FI-LO. FI-LO has the smallest centered RMSE in all the sites.

$RMSE_{SSO}$ are the smallest compared to $RMSE_{DPR}$, $RMSE_{SSO\_AVG}$ and $RMSE_{MSO}$ for all the sites (Table 7). $RMSE_{DPR}$ ranges from 39.56 to 153.9 mg m^{-2} d^{-1}, whereas $RMSE_{SSO}$ is much smaller and shows a narrower range from 11.23 to 46.67 mg m^{-2} d^{-1}. The mean of $RMSE_{SSO\_AVG}$ (ranges from 22.4 to 58.47 mg m^{-2} d^{-1}) over the sites is larger than the mean of $RMSE_{MSO}$ (ranges from 13.27 to 47.64 mg m^{-2} d^{-1}). The $RMSE_{DPR}$ of FI-SI is the biggest in all the sites and it reduces from 153.9 mg m^{-2} d^{-1} to 21.73 mg m^{-2} d^{-1} in the $RMSE_{SSO}$ which shows the biggest difference in all the sites. The $RMSE_{DPR}$ of CA-WP1 is the smallest in all the sites and it reduces from 39.56 to 20.31 in the $RMSE_{SSO}$. The $RMSE_{MSO}$ is larger than the $RMSE_{SSO\_AVG}$ at the FI-SI, SE-DE and CA-WP1 sites. However, when $RMSE_{SSO}$ is used as a reference

Table 6
Biases (mg m^{-2} d^{-1}) and correlation coefficients (R) of methane emissions between observation and simulations using default parameter (DPR) values, and simulations using parameter values from the single site optimization (SSO), averages of single site optimization (SSO_AVG) and multi-site optimization (MSO).

		FI-SI	FI-LO	SE-DE	PL-KO	CA-WP1	CA-MER
BIAS	DPR	96.29	0.48	36.66	48.64	25.62	121.56
	SSO	−3.37	8.65	7.49	−4.01	−2.97	−1.82
	SSO_AVG	0.56	−38.98	−9.58	2.73	−15.77	16.71
	MSO	4.08	−27.12	−4.91	3.1	−23.42	−1.87
R	DPR	0.84	0.87	0.66	0.29	−0.22	0.39
	SSO	0.85	0.90	0.73	0.45	0.33	0.47
	SSO_AVG	0.85	0.90	0.71	0.34	0.08	0.4
	MSO	0.83	0.89	0.69	0.42	−0.03	0.32

Table 7
Discrepancies between observed and simulated methane emissions (mg m^{-2} d^{-1}) are quantified by the root mean square error (RMSE). $RMSE_{DPR}$, $RMSE_{SSO}$, $RMSE_{SSO\_AVG}$ and $RMSE_{MSO}$ is calculated from simulations using default parameter (DPR) values, and simulations using parameter values from single site optimization (SSO), averages of single site optimization (SSO_AVG) and multi-site optimization (MSO).

	FI-SI	FI-LO	SE-DE	PL-KO	CA-WP1	CA-MER	mean
$RMSE_{DPR}$	153.9	47.91	86.08	99.43	39.56	136.2	96.83
$RMSE_{SSO}$	21.73	31.67	25.91	46.67	20.31	11.23	23.63
$RMSE_{SSO\_AVG}$	22.4	58.47	27.44	49.84	26.52	24.27	34.82
$RMSE_{MSO}$	25.40	42.56	28.07	47.64	31.73	13.27	29.21

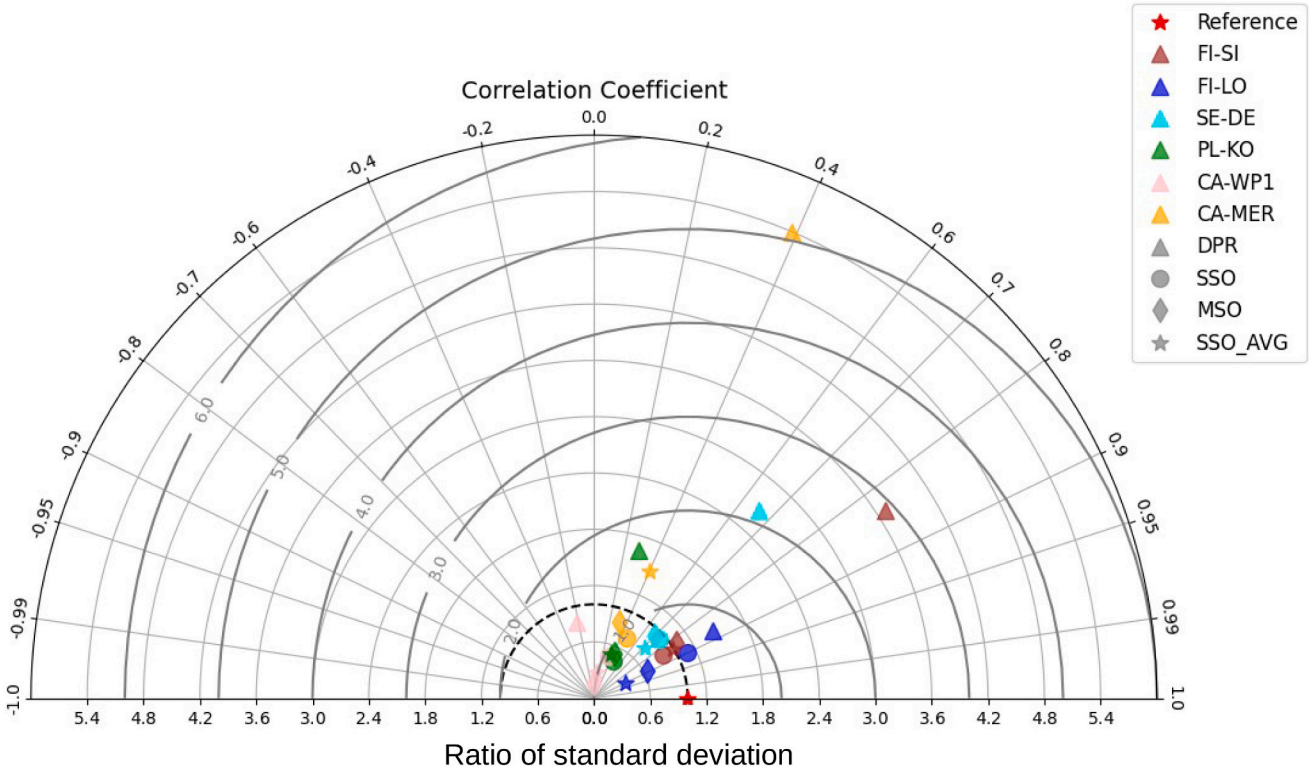

Fig. 8. Taylor diagrams of daily CH4 emissions. Statistics were calculated using simulated and observed daily CH4 emissions. All points were normalized by dividing the standard deviation of model results by the standard deviation of the corresponding measurements; thus, the reference point of ratio of standard deviation is 1.0. Sites are represented with different color. Simulations using parameter values from the default parameter (DPR), single site optimization (SSO), averages of single site optimization (SSO_AVG) and multi-site optimization (MSO)) are represented with different shapes.

point, $RMSE_{MSO}$ performs more stable than $RMSE_{SSO\_AVG}$ over the studied sites. More specifically, $RMSE_{SSO\_AVG}$ are much larger than $RMSE_{SSO}$ and $RMSE_{MSO}$ at FI-LO and CA-MER. Moreover, the simulated and observed CH_4 emission of CA-MER showed higher correlation coefficient and lower RMSE compared to CA-WP1 in the MSO simulations, although CA-MER and CA-WP1 were not included in the MSO.

The minimization efficiency (EF), which indicates the relationship between the DPR simulation and the simulations with optimized parameters, is calculated as 1-($RMSE_{SSO/SSO\_AVG/MSO}$/$RMSE_{DPR}$). The EF of FI-SI and CA-MER of the SSO, SSO_AVG and MSO simulations are larger than 0.8, while EF of FI-LO is the smallest (0.34 for SSO, −0.22 for SSO_AVG and 0.11 for MSO) in the sites (Table 8). The EF for SE-DE and PL-KO of SSO, SSO_AVG and MSO are larger than 0.5. Moreover, the normalized root mean square error (NRMSE) is defined by the RMSE

Table 8
Minimization efficiency of the simulations using the parameter values from the single site optimization (EF_{SSO}), averages of single site optimization (EF_{SSO_AVG}) and multi-site optimization (EF_{MSO}). EF are indicated by the relationship between the DPR simulation and simulation using optimized parameter values as 1- ($RMSE_{OPT}$/$RMSE_{DPR}$). Normalized root mean square error (NRMSE) is defined by the RMSE normalized by the mean of observed methane emissions. $RMSE_{DPR}$, $RMSE_{SSO}$ and $RMSE_{MSO}$ is calculated from simulations using default parameter (DPR) values, and simulations using parameter values from single site optimization (SSO), averages of single site optimization (SSO_AVG) and multi-site optimization (MSO).

	EF_{SSO}	EF_{SSO_AVG}	EF_{MSO}	$NRMSE_{DPR}$	$NRMSE_{SSO}$	$NRMSE_{SSO\_AVG}$	$NRMSE_{MSO}$
FI-SI	0.86	0.85	0.83	3.50	0.49	0.51	0.58
FI-LO	0.34	−0.22	0.11	0.80	0.53	0.98	0.71
SE-DE	0.70	0.68	0.67	2.15	0.69	0.68	0.70
PL-KO	0.53	0.50	0.52	3.38	1.59	1.70	1.62
CA-WP1	0.49	0.33	0.20	1.3	0.67	0.87	1.04
CA-MER	0.92	0.82	0.90	8.49	0.70	1.51	0.83

normalized by the mean of observed methane emissions. The $NRMSE_{SSO}$, $NRMSE_{SSO\_AVG}$ and $NRMSE_{MSO}$ of FI-SI are the smallest, whereas the $NRMSE_{SSO}$, $NRMSE_{SSO\_AVG}$ and $NRMSE_{MSO}$ of PL-KO are the largest in all the sites.

4. Discussion

4.1. Impact from optimized parameters on simulated methane emissions

Optimizing the model leads to a decreased production of CH_4 from the anoxic Rs at all the sites, due to decreased f_m compared to its default value. The value of f_m is dependent on the magnitude of the input anoxic Rs. The default value of f_m (0.5) was found to fit reasonably well with the estimated anoxic Rs in Raivonen et al. (2017), as the estimated anoxic Rs was smaller in magnitude than the anoxic Rs estimated by JULES in this work. Both $V_{O_{10}}$ and $V_{R_{10}}$ increased at most sites after optimization. The increase in $V_{O_{10}}$ suggests that the role of methane loss by oxidation could be greater than assumed using the default value (Eq. A8), while the increased $V_{R_{10}}$ might be compensating for the effects of the increased $V_{O_{10}}$ due to the competition of oxygen. In the model, the amount of oxidized CH_4 is strongly linked to $V_{O_{10}}$. The fraction of oxidized CH_4 in the produced CH_4 in the rhizosphere is 40 % and 56 % averaged over all the sites in the SSO and MSO simulations, respectively. These numbers are very close to the fixed values that have been set for the fraction of oxidized CH_4 in the rhizosphere globally in previous models, which is 40 % in Zhuang et al. (2004) and 50 % in Wania et al. (2010) respectively.

In HIMMELI, the substrate for CH_4 production, anoxic Rs, is allocated depth-wise according to the root density distribution, whose form is determined by λ_{root} (Eq. A5). λ_{root} affects both the allocation of anoxic Rs in the column and the depth to which plant transport reaches. A larger λ_{root} will facilitate the emission of CH_4 produced in deeper soil. The optimized results showed lower λ_{root} in the SSO than the default values in the studied sites, except for PL-KO. This means root depth is decreased for the studied sites except for PL-KO. On the contrary, a_{mA} increased for all the sites in the SSO compared to its default value which means an increase in the root ending area for root conductance. Moreover, τ showed increases in most of the sites but decreases for CA-WP1 and CA-MER. The increased τ represents a decrease in root conductance. The increase of a_{mA} and decrease of λ_{root} may compensate each other. The relatively high a_{mA} and low τ at CA-WP1 and CA-MER indicate that the optimized model tends to enhance plant transport capabilities at these two sites more than at other sites. This might be due to the low LAI used in the simulations at those two sites. The decrease of $f_{D,a}$ and $f_{D,w}$ at most sites, except CA-WP1 and CA-MER, indicates a decreased diffusion rate. Diffusion takes the major fraction (77 %) of the total CH_4 emission at CA-WP1 in the SSO simulation. This is because, in the SSO, $f_{D,a}$ is very high, while λ_{root} is small and WTD is low (except from May to June) at CA-WP1.

4.2. Simulated methane emissions

In the SSO simulations, the optimized model improved the explanation of variation in CH_4 emissions for all the sites. It performs relatively well at FI-SI, FI-LO and SE-DE sites with the correlation coefficient between modelled and measured CH_4 emissions larger than 0.7, while smaller than 0.5 at PL-KO, CA-WP1 and CA-MER sites. The differences between the measured and the simulated WTD and soil temperature for driving HIMMELI model are considered as the main reason for the discrepancies between the observed and simulated CH_4 emissions. In previous studies, temperature has been considered as the most influential factor for methanogenesis, while oxidation and plant transport dominant the methane emissions (van Huissteden et al., 2009; Riley et al., 2011). Smith et al. (2003) suggested that methanotrophy is more sensitive to soil moisture than soil temperature, and there is a clear relationship between methane oxidation rate and gas diffusivity. In most of the years at the studied sites in this work, the peaks of the modelled CH_4 emissions nicely match with observations. However, mismatches of peaks do exist, such as in year 2016, 2017 and 2018 of PL-KO, year 2018 of SE-DE, and year 2012 of CA-MER. In those years, the CH_4 emission peaks occurred when WTD was relatively high, but the temperature had risen enough for an intensive methanogenesis. The input WTD for HIMMELI showed a delayed drawdown with less extent at those years compared to observation, meanwhile, the warming up of the soil is delayed in the model. The delayed peaks in the simulated CH_4 emission could be mainly due to the later warming up of the soil (Fig. S1). Moreover, there are quite large deviations between the observed and simulated CH_4 emissions in 2013 and 2014 of PL-KO. In the observation, the high CH_4 emissions in 2013 and 2014 at PL-KO are mainly due to the high WTD, compared to the following years. In the following years, the general drawdown of WTD strongly limited the temperature driven CH_4 emission at this site (Fortuniak et al., 2021). Such differences are not shown in the simulated CH_4 emission at PL-KO, as the bias corrected WTD in those two years does not show significant differences to the WTD in the following years. Nevertheless, the effect from low WTD on CH_4 emission can be found in the year 2006, 2009 and 2018 of FI-SI, and the year 2015 of PL-KO, where lower WTD leads to lower CH_4 emission in both observation and the SSO simulation. It has been illustrated that HIMMELI performs well during dry seasons which can be directly attributed to the depth-wise distribution of CH_4 substrate according to the root density profile (Susiluoto et al., 2018).

The multi-year averaged fraction of plant transported CH_4 in the total CH_4 emission ranges from 22 % to 70 % across the studied sites. Wania et al. (2010) simulated CH_4 emissions for seven boreal peatland sites and found that the fraction of plant transported CH_4 ranged from 68 % to 85 %. Susiluoto et al. (2018) showed an even higher fraction of plant transport, ranging from 75 % to 95 %, when optimizing HIMMELI for FI-SI. Nevertheless, the proportion of seasonally variable plant transport was found to be between 7 % and 41 % at FI-SI fen based on chamber measurement from May to October of 2014 (Korrensalo et al., 2022). Salmon et al. (2022) found that plant mediated transport plays a major role, from 52 % to higher than 98 %, in the simulated methane emission flux over 14 northern peatlands. In our results, plant transport also takes the biggest fraction in the three transport ways of CH_4 from soil to atmosphere, when averaging over all the sites. The averaged fraction of plant transported CH_4 over sites is 54 % and 50 % in the SSO simulation and MSO simulation, respectively. Besides, the averaged fraction of diffusion over sites is 42 % for both SSO and MSO simulations, while the averaged fraction of ebullition over sites is 6 % and 8 % in the SSO simulation and MSO simulation, respectively. Despite the proportions of the amount of methane transported through diffusion, plant transport and ebullition to the total methane emission show large differences between sites, the averaged proportions of the three transport ways in the SSO and MSO simulations are similar. Seasonally, in the SSO simulation, plant transport dominates the CH_4 emission in winter simulations except for CA-WP1, whereas diffusion dominates the CH_4 emission in summer except for FI-LO and SE-DE. At FI-LO and SE-DE, plant transport dominates the CH_4 emission in summer. This is different to the model results shown in Salmon et al. (2022), where diffusion plays the major role in winter and plant transport is the main way in spring and summer over all the 14 studied peatland sites. Sun et al. (2012) found that plant transported CH_4 accounted for 38 % and 84 % of the total CH_4 emissions in the growing season and the surface soil freezing period, based on chamber measurements in a temperate marsh site in China. The high fraction of CH_4 transported through plant in the surface soil freezing period was explained with the reason that CH_4 diffusion was blocked and accumulated under the frozen surface and compelled to diffuse through vascular plants from the soil to atmosphere. However, as there is no ice or snow covering effects on CH_4 emission considered in HIMMELI, the high fraction of plant transport in winter in our simulation results can be attributed to the high input LAI

values in winter (Raivonen et al., 2017), despite the differences between summer and winter LAI values at the sites have already widened after bias correction.

Ebullition to the surface takes a small fraction (from 0 to 3.5 %) of the total CH_4 emission at our studied sites, except for FI-LO. The amount of ebullition at FI-LO reaches 23 % and 40 % of the CH_4 emission in the SSO and MSO simulations, respectively. The higher fraction of ebullition to the surface at FI-LO is mainly due to the longer time period of above surface WTD compared to other studied sites. The amount of ebullition varies largely between different sites. Kaiser et al. (2017) found high ebullition fluxes for a polygonal tundra in the Siberian permafrost region by process-based modelling, where the ice-free soil layer reaches only about 30 cm depth during summer. However, there was almost no ebullition to the surface in the simulation results of seven boreal peatlands in Wania et al. (2010). Susiluoto et al. (2018) found approximately 0 to 3 % of the total CH_4 flux is ebullition from the model simulation at the FI-SI site. This is almost in line with the fraction of ebullition at FI-SI in our study, which is 1.9 % in the SSO simulation and 3.4 % in the MSO simulation. In Salmon et al. (2022), there were quite some ebullition in 2013 and 2014 at PL-KO, however, this is not shown in our results. This is because the model schemes are different and the underestimated WTD of 2013 and 2014 at PL-KO in HIMMELI input. In HIMMELI, ebullition happens when the sum of the partial pressures of dissolved gases is larger than the sum of atmospheric and hydrostatic pressures in the water column (see Eq. A16); Also, when WTD is below ground, ebullition happened below WTD is transferred to diffusion at the first air-filled peat layer above the water table level in the model. Therefore, ebullition to the surface in HIMMELI happens at times when there is sufficient amount of CH_4 in the water column and the WTD reaches or above the surface.

The averages of the methane emissions estimated from the studied sites can be used to roughly estimate the CH_4 emissions of northern wetlands. The area of the inundated and non-inundated vegetated northern wetlands, located in the north of 30°N, is estimated to be in the range of 1.6 Mkm^2 as the annual mean minimum to 4.3 Mkm^2 as the annual mean maximum in the Global Wetland Area and Dynamics for Methane Modelling (WAD2M) version 1.0 dataset (Z. Zhang et al., 2021). The annual methane emission of northern wetlands estimated based on the averaged CH_4 emissions from the studied sites of the SSO and MSO simulations and the annual mean minimum and maximum wetland areas in WAD2M is in the range of 20.0–53.8 and 15.2–40.9 Tg CH_4 yr^{-1}, respectively. By applying the northern peatland extent estimated in previous studies (Qiu et al., 2019; Xu et al., 2018; Batjes, 2016; Joosten, 2009; Lehner and Döll, 2004), which is between 2.832 Mkm^2 and 3.896 Mkm^2, the annual CH_4 emission of northern wetlands is 35.5–48.8 and 27.0–37.1 Tg CH_4 yr^{-1} according to the SSO simulation and MSO simulation, respectively. The annual methane emissions of northern wetlands estimated in this work are in agreement with the estimations in other studies. The computed methane emission over northern wetlands averaged in the period of 2010–2019 is around 21.5–93 Tg CH_4 yr^{-1} from bottom-up approaches (i.e., biogeochemical models) (Saunois et al., 2024). In Qiu et al. (2022), the simulated CH_4 emissions of northern peatlands by five state-of-the-art peatland models were bias-corrected with observations and showed the present-day CH_4 emissions for northern peatlands to be 26–32 Tg CH_4 yr^{-1}. By upscaling flux measurements with random forest algorithm, the wetland methane emission in the north of 45°N was estimated to be between 30.6 and 37.6 Tg CH_4 yr^{-1} depends on different wetland maps (Peltola et al., 2019).

4.3. Possible improvements in the JULES-HIMMELI model

The simulated methane emission has significant improvement in the SSO and MSO simulation compared to the DPR simulation. Nevertheless, the simulated methane emission by HIMMELI could possibly be further improved with more accurate driving variables modelled by the land surface model JULES or more detailed description of the methane production and emission processes in the peatland methane emission model HIMMELI.

As analyzed in previous sections, the input data have a role in affecting the modelled methane. Although we have bias corrected the WTD and LAI simulated by JULES for driving HIMMELI, differences to observations still exist. For the annual maximum LAIs derived from the Sentinel-2 satellite data, there might be uncertainties in the LAI deriving algorithm and atmospheric correction, and also selection of representative area. Moreover, the minimum LAI in winter is not bias corrected due to the lack of measurement. The biases in LAI can impact the transport capability of both CH_4 and O_2 in peat column in HIMMELI. Overall, when using JULES to provide the driving conditions to HIMMELI, more realistic representations of peat soil carbon and peat hydrology processes, especially WTD, and wetland PFTs, are needed in JULES to improve the simulated wetland CH_4 emissions. Chadburn et al. (2022) has developed a new approach in simulating peat dynamics (accumulation, degradation and stability) in the vertically resolved soil carbon scheme in JULES. More realistic simulation of anoxic respiration, which is the substrate for CH_4 production in HIMMELI, can improve the magnitude and annual pattern of CH_4 emissions (Raivonen et al., 2017). Moreover, distributed representation of WTD may also be simulated in JULES by the microtopography and ponding scheme developed in Smith et al. (2022), but this would require data about the fine structure and heterogeneity of the wetland. Also, soil moisture and soil temperature are closely linked. Soil temperature can not only impact the reaction speed, e.g. CH_4 oxidation in the soil, but also solubility of gases in the soil. Those more advanced schemes could be tested in the JULES-HIMMELI model in the future. In addition, it has been proved that peatland PFTs that capture multiple plant traits are powerful in explaining peatland CO_2 and CH_4 flux variability (Laine et al., 2022). Adding peatland PFTs with the specific traits of peatland plants in JULES would be useful for a more realistic representation of peatland vegetation and carbon dynamics. In HIMMELI, higher LAI means higher transport capacity of gases, e.g. CH_4 and O_2, of the plant. O_2 concentration in the peat can impact both the inhibition of CH_4 production and CH_4 oxidation, which is an important player in simulating CH_4 emission. However, observed O_2 data in peat soil for validation are largely lacking and expected to be included in future observations. Furthermore, the snow and ice covering effect on methane emission is under development in HIMMELI. Methane could be diffused to snowpack covering the peatland or accumulated in gas bubbles under ice in winter, and released in spring simultaneously with snow melting (Mastepanov et al., 2013; Sriskantharajah et al., 2012). Those processes could reduce the CH_4 emission in winter and lead to CH_4 emission bursts in spring, which are considered necessary when simulating CH_4 emissions in northern peatlands.

5. Conclusions

A process-based peatland methane emission model HIMMELI was integrated with a current state-of-art land surface model JULES in this work. An evaluation of the JULES-HIMMELI model was performed with ten model parameters optimized with site level measurements at six northern wetland sites separately (i.e., single site optimization) or together (i.e., multi-site optimization). The default wetland methane emission scheme in JULES only takes into account CH_4 emissions from saturated wetlands in a simple way, while HIMMELI simulates CH_4 production, oxidation and transportation by vascular plants, ebullition and diffusion in a vertical soil column.

There is a significant improvement in the modelled CH_4 emissions when using optimized parameter values. Results show that CH_4 emission estimated from the DPR simulation is overestimated by 54.88 mg m^{-2} d^{-1} (20.03 g m^{-2} yr^{-1}) on average over the studied sites compared to the measurement. Averaged over sites, the overestimation of CH_4 emissions in the DPR simulation is reduced to −0.70 mg m^{-2} d^{-1} (−0.26 g m^{-2} yr^{-1}) in the SSO simulation, and −7.39 mg m^{-2} d^{-1} (−2.70 g m^{-2} yr^{-1})

and −8.36 mg m^{-2} d^{-1} (−3.05 g m^{-2} yr^{-1}) in the SSO_AVG simulation and MSO simulation, respectively. However, the RMSEs between the simulated and observed methane emissions of MSO simulations are more stable than SSO_AVG simulations at the studied sites, when the RMSEs of SSO simulations are used as reference points. This finding suggests that the optimized parameter values obtained from MSO should provide methane emission estimation with lower uncertainties than those derived from SSO_AVG when using the JULES-HIMMELI model to simulate methane emissions in the northern wetlands. In addition, no significant impact on simulated CH_4 emissions from bog or fen in the MSO simulations is shown. However, to further reduce the uncertainties, future studies could increase the number of wetlands sites with flux data and group them into different sub-groups, such as bog and fen, when using MSO to derive the model parameter values.

In the optimized JULES-HIMMELI model, a much smaller proportion of anoxic respiration is used to produce CH_4 compared to the DPR simulation, and the fraction of oxidized CH_4 in the produced CH_4 in the rhizosphere is consistent with previous studies. Averaged over sites, plant transport accounts for 54 % and 50 % of the total CH_4 emissions in the SSO and MSO simulations, respectively. Meanwhile, the fraction of diffusion is 42 %, and the fraction of ebullition is 6 % in the SSO simulation and 8 % in the MSO simulation. In the SSO simulations, plant transport dominates the CH_4 emission during winter, while diffusion dominates the CH_4 emission in summer at most sites. The high fraction of plant transport in the total CH_4 emission in winter is due to the high winter LAI simulated by JULES, which needs to be corrected in future work. The high fraction of ebullition of FI-LO site is due to the long period of above surface WTD. The discrepancies between the model and measured CH_4 emissions can be mainly attributed to the uncertainties of the HIMMELI input data (i.e. WTD and soil temperature), which are model quantities simulated by JULES, and the missing processes in HIMMELI model scheme. Thus, enhancing model development on peat soil carbon and hydrology processes, and incorporating wetland plant functional types in JULES, as well as accounting for the snow and ice covering effect in HIMMELI could improve the accuracy of simulated wetland CH_4 emissions by the JULES-HIMMELI model.

Supplementary data to this article can be found online at https://doi.org/10.1016/j.scitotenv.2025.179526.

CRediT authorship contribution statement

Yao Gao: Writing – original draft, Visualization, Validation, Methodology, Investigation, Funding acquisition, Formal analysis, Data curation, Conceptualization. **Eleanor J. Burke:** Writing – review & editing, Methodology, Data curation. **Sarah E. Chadburn:** Writing – review & editing, Methodology. **Maarit Raivonen:** Writing – review & editing, Methodology. **Tiina Markkanen:** Writing – review & editing, Supervision. **Mika Aurela:** Data curation. **Lawrence B. Flanagan:** Data curation. **Krzysztof Fortuniak:** Data curation. **Elyn Humphreys:** Data curation. **Annalea Lohila:** Data curation. **Tingting Li:** Writing – review & editing. **Ivan Mammarella:** Data curation. **Olli Nevalainen:** Data curation. **Mats B. Nilsson:** Data curation. **Włodzimierz Pawlak:** Data curation. **Aki Tsuruta:** Writing – review & editing. **Huiyi Yang:** Software. **Tuula Aalto:** Writing – review & editing, Supervision, Project administration, Conceptualization.

Declaration of Generative AI and AI-assisted technologies in the writing process

Some of the text of this manuscript has been proofread using ChatGPT during the preparation. After using this tool/service, the authors reviewed and edited the content as needed and take full responsibility for the content of the published article.

Financial support

This work is mainly supported with the funding from the European Union's Horizon 2020 research and innovation programme under grant agreement 641816 (CRESCENDO) and the Maj ja Tor Nessling Foundation through the project "Resilience of high-latitude wetlands in a changing climate: modelling and evaluation of wetlands carbon sequestration and methane emissions" (Project number: 202000476). We would also like to thank the Strategic Research Council at the Research Council of Finland (STN-SOMPA, 336573, STN-MULTA, 352431), Ministry of Agriculture and Forestry of Finland Grant No. 4400T-2105 (TURNEE), Research Council of Finland Grants No. 341752 and 341753 (RESPEAT), 312932 (SOMPA), 350184 (WINMET), 337552 (ACCC), EU-HORIZON ALFAWETLANDS (No. 101056844), EU-HORIZON ESM2025 (No. 101003536), EU-Horizon EYE-CLIMA (No. 101081395), EU-HORIZON WetHorizons (No. 101056848), EU-LIFE21-CCM-LV-LIFE PeatCarbon (No. 101074396), funding from ICOS-Finland (University of Helsinki), and Business Finland Grant no. 6905/31/2018 for financial support. Funding for research in Kopytkowo, Poland was provided by the National Science Centre, Poland under project UMO-2020/37/B/ST10/01219 and University of Lodz under project 4/IDUB/DOS/2021.

Declaration of competing interest

The authors declare that they have no known competing financial interests or personal relationships that could have appeared to influence the work reported in this paper.

Acknowledgments

Olli Peltola is acknowledged for preparing the daily methane flux data from the original site measured data. Antti Leppänen and Jouni Susiluoto is acknowledged for giving instructions on using HIMMELI.

Appendix A. HIMMELI model description

1. HIMMELI model equations

The equations of the HIMMELI model can be introduced as the following four parts: the governing equations, methane (CH_4) production, CH_4 oxidation and aerobic respiration, CH_4 transport.

1) Governing equations

The concentration of CH_4, carbon dioxide and oxygen (C_{CH_4}, C_{CO_2} and C_{O_2}) at depth z are governed by the equations:

$$\frac{\partial C_{CH_4}(t,z)}{\partial t} = R_{CH_4,pro} - R_{CH_4,oxid} - F_{diff,CH_4} - F_{plt,CH_4} - F_{ebu,CH_4} \quad (A.1)$$

$$\frac{\partial C_{O_2}(t,z)}{\partial t} = -R_{aR} - 2R_{CH_4,oxid} - F_{diff,O_2} - F_{plt,O_2} - F_{ebu,O_2} \quad (A.2)$$

$$\frac{\partial C_{CO_2}(t,z)}{\partial t} = R_{anR} - R_{CH_4,pro} + R_{CH_4,oxid} + R_{aR} - F_{diff,CO_2} - F_{plt,CO_2} - F_{ebu,CO_2} \quad (A.3)$$

Here, $R_{CH_4,pro}$ is the CH_4 production rate; $R_{CH_4,oxid}$ is the CH_4 oxidation rate; R_{anR} is the rate of anaerobic respiration; R_{aR} is the rate of aerobic peat respiration; $F_{diff,X}$, $F_{plt,X}$ and $F_{ebu,X}$ are the transport rate of gas X of diffusion, plant transport and ebullition, respectively.

2) CH_4 production

The CH_4 production rate $R_{CH_4,pro}$ in the peat layer at depth z is calculated as below:

$$R_{CH_4,pro} = f_m R_{anR(z)} \frac{1}{1 + \eta C_{O_2}(z)} \quad (A.4)$$

where f_m is the fraction of anaerobic respiration becoming methane; η is a parameter representing the sensitivity of methanogenesis to O_2 inhibition. Thus, in the circumstance with no O_2, the CH_4 production rate is called potential methane production rate. $R_{anR(z)}$ here is the rate of anaerobic respiration at depth z, which is calculated as:

$$R_{anR}(z) = \frac{V_{anR}}{dz} f_{root,an}(z) \quad (A.5)$$

Here, V_{anR} is the input anaerobic respiration; dz is the layer thickness; $f_{root,an}(z)$ is the ratio of root mass at depth z to the total root mass of the anaerobic zone. The formulation of $f_{root}(z)$ is adopted from Wania et al. (2010):

$$f_{root}(z) = Cexp\left(\frac{-z}{\lambda}\right) \quad (A.6)$$

λ is a root depth distribution decay parameter, and C is a normalizing constant for making the sum of root fractions equals 1.

3) CH_4 oxidation and aerobic respiration

The rate of CH_4 oxidation at depth z ($R_{CH_4,oxid}(z)$) is assumed to follow the dual-substrate Michaelis-Menten kinetics (Arah and Stephen, 1998):

$$R_{CH_4,oxid}(z) = V_o(z) \frac{C_{o_2}(z)}{K_{o_2} + C_{o_2}(z)} \times \frac{C_{CH_4}}{K_{CH_4} + C_{CH_4}} \quad (A.7)$$

where $V_o(z)$ is the potential oxidation rate at depth z; k_{O_2} and k_{CH_4} are the Michaelis-Menten constants for O_2 and CH_4, respectively. The calculation of $V_o(z)$ follows Arrhenius equation:

$$V_O(z) = V_{o_{10}} exp\left(\frac{\Delta E_{oxid}}{R}\left(\frac{1}{283} - \frac{1}{T(z)}\right)\right) \quad (A.8)$$

Here, $V_{O_{10}}$ is the CH_4 oxidation rate at temperature 10 °C; ΔE_{oxid} is the activation energy of the oxidation reaction; R is the universal gas constant; $T(z)$ is the temperature at depth z.

The rate of aerobic peat respiration at depth z ($R_{aR}(z)$) is also described with a Michaelis-Menten model:

$$R_{aR}(z) = V_R(z) \frac{C_{O_2}(z)}{K_R + C_{O_2}(z)} \quad (A.9)$$

where $V_R(z)$ is the potential aerobic respiration rate of peat at depth z; k_R is the Michaelis-Menten constant for the reaction. $V_R(z)$ is also calculated with Arrhenius equation:

$$V_R(z) = V_{R_{10}} exp\left(\frac{\Delta E_R}{R}\left(\frac{1}{283} - \frac{1}{T(z)}\right)\right) \quad (A.10)$$

Here, $V_{R_{10}}$ is the rate of aerobic respiration of peat at temperature 10 °C; ΔE_R is the activation energy of aerobic respiration.

4) CH_4 transport

The diffusion rate of gas X is calculated as:

$$F_{diff,X} = D_{medium,x} \frac{\partial C_{X,medium}}{\partial z} \quad (A.11)$$

where $D_{medium,X}$ is the diffusion coefficients in a medium, which is air-filled peat or water-filled peat here. $C_{x,medium}$ is the concentration of gas X in the medium. The diffusion coefficient of gas X in air-filled peat ($D_{peat_{air},X}$) and water-filled peat ($D_{peat_{water},X}$) are calculated by multiplying the diffusion rate of gas X in free-air ($D_{air,X}$) or free-water ($D_{water,X}$) by the constant reduction factors in air-filled peat ($f_{D,a}$) or water-filled peat ($f_{D,w}$) (Eq. 12 and 13).

$$D_{peat_{air},X} = f_{D,a} D_{air,X} \quad (A.12)$$

$$D_{peat_{water},X} = f_{D,w} D_{water,X} \quad (A.13)$$

When the diffusion flux across the water-air interface, the flux is calculated from the difference of concentration in the water-filled ($C_{x,water}$) and air-filled ($C_{x,air}$) layers following Bird et al. (1960) (Eq. 14). $k_{H,X}$ is the Henry's law coefficient in dimensionless form.

$$F_{diff,water_{air},X} = \frac{2 D_{peat_{water},X} D_{peat_{air},X}}{D_{peat_{air},X} + D_{peat_{water},X} k_{H,X}} \frac{C_{x,water} - k_{H,X} C_{X,air}}{dz} \quad (A.14)$$

The plant transport rate of gas X is calculated as eq. (15) following the formulation from Stephen et al. (1998):

$$F_{plt,X} = \frac{\varepsilon_r(z) D_{peat_{air},X}}{\tau} \frac{C_x(z,t) - C_{atm,X}}{z} \quad (A.15)$$

where $\varepsilon_r = a_{mA} \frac{f_{root}(z)}{dz} \frac{LAI}{SLA}$, is the density of cross-sectional area of root endings at depth z ($m^2 m^{-3}$) and τ is root tortuosity; $C_{atm,X}$ is the atmospheric partial pressure of gas X; LAI is the vegetation leaf area index, given as input; SLA is specific leaf area.

The ebullition rate of gas X is calculated as:

$$F_{ebu,X} = -k\sigma \frac{pp_X}{RT} \frac{\sum_X PP_x(z) - \left(P_{atm} + P_{hyd}(z)\right)}{\sum_X pp_X(z)} \quad (A.16)$$

Here, pp_x refers to the partial pressure of gases X; k is an ebullition rate constant; σ is peat porosity; R is the universal gas constant; P_{atm} is the atmospheric pressure and is the hydrostatic pressure at depth z.

2. Bug corrections

Three small errors that were found in the original HIMMELI code (doi:https://doi.org/10.5194/gmd-10-4665-2017-supplement) had been corrected before the present work. These errors were:

1) In the calculation of how dissolved O_2 inhibits CH_4 production, O_2 concentration was not normalized with layer thickness in the original version.

2) In HIMMELI, an extra (peat) layer is added in the background layer structure whenever the input WTD is not at the border of two layers. This enables using the exact daily WTD in the simulation. However, in some cases, the exact WTD cannot be used (e.g. when it is <1 cm distance from a background layer border) but it is rounded to the nearest background layer boundary. In the original code, this possible rounding was not taken into account when allocating daily soil temperatures.

3) The air temperature used when converting ambient mixing ratios to mol m^{-3} was not updated with daily input temperatures.

Appendix B. Site descriptions

1) Siikaneva

The Siikaneva site (61.8°N, 24.2°E) is a boreal oligotrophic fen site located in Ruovesi in southern Finland (Rinne et al., 2007). The peat depth at the site is from 2 to 4 m. The dominant vegetation of the site includes sedges (*C. rostrata*, *C. limosa*, *E. vaginatum*), Rannochrush (*Scheuchzeria palustris*) and peat mosses (*Sphagnum balticum*, *S. majus*, and *S. papillosum*). The annual mean temperature of 3.3 °C and precipitation of 713 mm have been measured at the nearest long-term weather station during the period 1971 to 2000 (Drebs et al., 2002). For a more detailed description of Siikaneva, see Aurela et al. (2007) and Rinne et al. (2007).

2) Lompolojänkkä

The Lompolojänkkä site (68.0°N, 24.2°E) is an open, pristine and nutrient-rich sedge fen located in northern Finland. The peat depth at the site is up to 3 m at the center of the fen. The vegetation layer at the site is relatively dense and dominated by *Betula nana*, *Menyanthes trifoliata*, *Salix lapponum* and Carex spp. with the mean vegetation height of 40 cm. The mean annual temperature averaged over the period 1971–2000 at the nearest long-term weather station is 1.4 °C (Pirinen et al., 2012). A small stream flows through the site and brings water to the site. The soil at this site is almost continuously saturated throughout the year. More detailed description of Lompolojänkkä can be found in Aurela et al. (2009); Lohila et al. (2010).

3) Degerö Stormyr

The Degerö Stormyr site (64.2°N, 19.6°E) is an undisturbed mixed acid mire system situated in the Kulbäcksliden Experimental Forest in Northern Sweden. The mire is situated on high land between two major rivers, the Umeälven and Vindelälven, approximately 70 km from the Gulf of Bothnia. The mire system is composed of interconnected smaller mires divided by islets and ridges of glacial till (Nilsson et al., 2008). The peat depth of the site is mainly between 3 and 4 m, but depths of 8 m have also been measured. The deepest peat depth corresponds to an age of 8000 years. The footprint of the measured CO_2 and methane fluxes is from a minerogenic oligotrophic mire. The vegetation is dominated by lawn (*S. balticum* Russ. C. Jens and *S. lindbergii* Schimp.) and carpet (*Sphagnum majus* Russ. C. Jens) plant communities, as well as vascular (*Eriophorum vaginatum* L., Trichophorum cespitosum (L.) Hartm., *Vaccinium oxycoccos* L., Andromeda polifolia L. and *Rubus chamaemorus* L., with both *Carex limosa* L. and Schezeria palustris L. occurring more sparsely) plant community.

4) Kopytkowo

The Kopytkowo site (53.6°N, 22.9°E) is a mire located in a large flat area of the Middle Biebrza Basin in northeastern Poland. The depth of peat in this area reaches 2.5 m. The soil of the mire around the site was slightly decomposed due to dehydration. The dominant vegetation around the site is a mixture of reeds, sedges and rushes. The wetlands of Biebrza National Park experienced melioration treatments in the 19th and 20th centuries. In the mid-nineteenth century, the wetlands first drained to intensify agriculture in the region. This human activity has caused partial degradation of the wetland peat and the natural succession to trees and shrubs was accelerated. In 1993, the Biebrza National Park was established, and restoration work has been conducted to restore the original hydrological conditions. The climate of northeastern Poland is temperate with continental influences, with relatively cold winters and warm summers. More detailed descriptions can be found at Fortuniak et al. (2017) and Fortuniak et al. (2021).

5) Western Peatland 1

The Western Peatland 1 site (55.0°N, −112.5°E) is an undisturbed moderately "rich" fen – rich in species richness, not nutrient availability (Flanagan and Syed, 2011). The area around the site is quite flat and with relatively homogeneous vegetation in around 1.5 to 2 km in all directions, except in the north where upland aspen forest shows in around 1 km away from the measurement site. The site is dominated by stunted trees (*Picea mariana* and *Larix laricina*), abundant tall shrubs (*Betula pumila*), and a wide range of moss species, including Sphagnum spp. (*S. angustifolium*, *S. fuscum*, and others), brown moss species (*Drepanocladus aduncus*, Aulocomium palustre, and others) and a feather moss species (*Pleurozium schreberi*). There are also several herbs and dwarf shrubs with aerenchyma tissue (*Triglochin maritima*, *Menyanthes trifoliata*, and Carex spp.) exist in the area. The total leaf area index for the site was 2.6 ± 0.16 m^2/m^2. The total ecosystem carbon stock is 51 kg C/m^2, which is dominated by carbon accumulated in below-ground peat. The above ground live plant tissue is only about 1 % of the total ecosystem carbon stock which is contributed by the two tree species. The mean annual temperature and precipitation at the nearest weather station were 2.1 °C and 504 mm averaged over 1971–2000. Detailed descriptions of vegetation and site characteristics were previously provided by Syed et al. (2006) and Long et al. (2010).

6) Mer Bleue

The Mer Bleue site (45.4°N, −75.5°E) is an undisturbed ombrotrophic bog located east of Ottawa, Canada. The peat depth of the site varies from 5 to 6 m at the center and 0.3 m at the edges. The surface of the area of the flux tower is dominated by hummock microtopography (75 % of the area) with approximately 25 cm between the tops of hummocks and inter-hummock spaces (Brown et al., 2014). The vegetation of the site is dominated by evergreen and deciduous shrubs, and Sphagnum mosses (Lafleur et al., 2005). The mean annual temperature is 6.4 ± 0.8 °C, and annual precipitation is 943 mm averaged over 1981–2010. The site has hosted a long-term carbon cycle research program since 1998. For more detailed site description, see Moore et al. (2002), Lafleur et al. (2003) and Roulet et al. (2007).

Data availability

The data generated and analyzed during the study is available by request from the corresponding author. The in-situ measurement data, including the CH_4 flux and meteorological data as well as other ancillary data can be requested from the site PIs. The CH_4 fluxes for the Siikaneva site can be obtained from the AVAA SmartSMEAR website (https://smear.avaa.csc.fi/download).The FLUXNET data used in this study can be accessed from the FLUXNET database (https://fluxnet.org/data/). The tool for deriving Sentinel-2 LAI data is in an open GitHub repository (https://github.com/ollinevalainen/satellitetools, doi:https://doi.org/10.5281/zenodo.5993292, Nevalainen, 2022). HIMMELI v1.0 model source code can be found in doi:https://doi.org/10.5194/gmd-10-4665-2017-supplement. JULES model code and the files for running it are available from the Met Office Science Repository Service: https://code.metoffice.gov.uk is required, and code is freely available subject to completion of a software license.

References

Aalto, T., Tsuruta, A., Mäkelä, J., Müller, J., Tenkanen, M., Burke, E., Chadburn, S., Gao, Y., Mannisenaho, V., Kleinen, T., Lee, H., Leppänen, A., Markkanen, T., Materia, S., Miller, P.A., Peano, D., Peltola, O., Poulter, B., Raivonen, M., Saunois, M., Wårlind, D., Zaehle, S., 2025. Air temperature and precipitation constraining the modelled wetland methane emissions in a boreal region in northern Europe. Biogeosciences 22, 323–340. https://doi.org/10.5194/bg-22-323-2025.

Arah, J.R.M., Stephen, K.D., 1998. A model of the processes leading to methane emission from peatland. Atmos. Environ. 32, 3257–3264.

Aurela, M., Riutta, T., Laurila, T., Tuovinen, J.-P., Vesala, T., Tuittila, E.-S., Rinne, J., Haapanala, S., Laine, J., 2007. CO_2 exchange of a sedge fen in southern Finland–the impact of a drought period. Tellus B 59, 826–837.

Aurela, M., Lohila, A., Tuovinen, J.P., Hatakka, J., Riutta, T., Laurila, T., 2009. Carbon dioxide exchange on a northern boreal fen. Boreal Environ. Res. 14, 699–710. https://doi.org/10.1093/treephys/tpn047.

Aurela, M., Lohila, A., Tuovinen, J.P., Hatakka, J., Penttilä, T., Laurila, T., 2015. Carbon dioxide and energy flux measurements in four northern-boreal ecosystems at Pallas. Boreal Environ. Res. 20, 455–473.

Batjes, N.H., 2016. Harmonized soil property values for broad-scale modelling (WISE30sec) with estimates of global soil carbon stocks. Geoderma 269, 61–68. https://doi.org/10.1016/J.GEODERMA.2016.01.034.

Best, M.J., Pryor, M., Clark, D.B., Rooney, G.G., Essery, R., Ménard, C.B., Edwards, J.M., Hendry, M.A., Porson, A., Gedney, N., Mercado, L.M., 2011. The Joint UK Land Environment Simulator (JULES), model description–part 1: energy and water fluxes. Geosci. Model Dev. 4 (3), 677–699.

Bird, R.B., Stewart, W.E., Lightfoot, E.N., 1960. Transport Phe- nomena. John Wiley and Sons, New York, USA.

Brown, M.G., Humphreys, E.R., Moore, T.R., Roulet, N.T., Lafleur, P.M., 2014. Evidence for a nonmonotonic relationship between ecosystem-scale peatland methane emissions and water table depth. J. Geophys. Res. Biogeosci. 119 (5), 826–835.

Burke, E.J., Ekici, A., Huang, Y., Chadburn, S.E., Huntingford, C., Ciais, P., Friedlingstein, P., Peng, S., Krinner, G., 2017. Quantifying uncertainties of permafrost carbon–climate feedbacks. Biogeosciences 14, 3051–3066.

Chadburn, S.E., Burke, E., Essery, R., Boike, J., Langer, M., Heikenfeld, M., Cox, P., Friedlingstein, P., 2015a. An improved representation of physical permafrost dynamics in the JULES land-surface model. Geosci. Model Dev. 8, 1493–1508. https://doi.org/10.5194/gmd-8-1493-2015.

Chadburn, S.E., Burke, E.J., Essery, R.L.H., Boike, J., Langer, M., Heikenfeld, M., Cox, P. M., Friedlingstein, P., 2015b. Impact of model developments on present and future simulations of permafrost in a global land-surface model. Cryosphere 9, 1505–1521. https://doi.org/10.5194/tc-9-1505-2015.

Chadburn, S., Krinner, G., Porada, P., Bartsch, A., Beer, C., Belelli Marchesini, L., Boike, J., Ekici, A., Elberling, B., Friborg, T., Hugelius, G., Johansson, M., Kuhry, P., Kutzbach, L., Langer, M., Lund, M., Parmentier, F.-J.W., Peng, S., Van Huissteden, K., Wang, T., Westermann, S., Zhu, D., Burke, E.J., 2017. Carbon stocks and fluxes in the high latitudes: using site-level data to evaluate Earth system models. Biogeosciences 14, 5143–5169. https://doi.org/10.5194/bg-14-5143-2017. https://www.biogeosciences.net/14/5143/2017/.

Chadburn, S.E., Aalto, T., Aurela, M., Baldocchi, D., Biasi, C., Boike, J., Burke, E.J., Comyn-Platt, E., Dolman, A.J., Duran-Rojas, C., Fan, Y., Friborg, T., Gao, Y., Gedney, N., Göckede, M., Hayman, G.D., Holl, D., Hugelius, G., Kutzbach, L., Lee, H., Lohila, A., Parmentier, F.-J., Sachs, T., Shurpali, N.J., Westermann, S., 2020. Modeled microbial dynamics explain the apparent temperature sensitivity of wetland methane emissions. Glob. Biogeochem. Cycles 34 (11).

Chadburn, S.E., Burke, E.J., Gallego-Sala, A.V., Smith, N.D., Bret-Harte, M.S., Charman, D.J., Drewer, J., Edgar, C.W., Euskirchen, E.S., Fortuniak, K., Gao, Y., Nakhavali, M., Pawlak, W., Schuur, E.A.G., Westermann, S., 2022. A new approach to simulate peat accumulation, degradation and stability in a global land surface scheme (JULES vn5.8_accumulate_soil) for northern and temperate peatlands. Geosci. Model Dev. 15, 1633–1657. https://doi.org/10.5194/gmd-15-1633-2022.

Chen, H., Xu, X., Fang, C., Li, B., Nie, M., 2021. Differences in the temperature dependence of wetland CO_2 and CH_4 emissions vary with water table depth. Nat. Clim. Chang. 11 (9), 766–771.

Clark, D.B., Mercado, L.M., Sitch, S., Jones, C.D., Gedney, N., Best, M.J., Pryor, M., Rooney, G.G., Essery, R.L.H., Blyth, E., Boucher, O., Harding, R.J., Huntingford, C., Cox, P.M., 2011. The Joint UK Land Environment Simulator (JULES), model description–part 2: carbon fluxes and vegetation dynamics. Geosci. Model Dev. 4 (3), 701–722. https://doi.org/10.5194/gmd-4-701-2011.

Comyn-Platt, E., Hayman, G., Huntingford, C., Chadburn, S.E., Burke, E.J., Harper, A.B., Collins, W.J., Webber, C.P., Powell, T., Cox, P.M., Gedney, N., Sitch, S., 2018. Carbon budgets for 1.5 and 2 C targets lowered by natural wetland and permafrost feedbacks. Nat. Geosci. 11, 568.

Dlugokencky, E.J., Bruhwiler, L., White, J.W.C., Emmons, L.K., Novelli, P.C., Montzka, S. A., Masarie, K.A., Lang, P.M., Crotwell, A.M., Miller, J.B., Gatti, L.V., 2009. Observational constraints on recent increases in the atmospheric CH_4 burden. Geophys. Res. Lett. 36 (18).

Dorodnikov, M., Knorr, K.H., Kuzyakov, Y., Wilmking, M., 2011. Plant-mediated CH_4 transport and contribution of photosynthates to methanogenesis at a boreal mire: a 14C pulse-labeling study. Biogeosciences 8 (8), 2365–2375.

Drebs, A., Nordlund, A., Karlsson, P., Helminen, J., Rissanen, P., 2002. Climatological Statistics of Finland 1971-2000, 99. Finnish Meteorological Institute, Helsinki. ISBN 951-697-568-2,.

Duan, Q., Sorooshian, S., Gupta, V.K., 1994. Optimal use of the SCE-UA global optimization method for calibrating watershed models. J. Hydrol. 158 (3-4), 265–284.

Flanagan, L.B., Syed, K.H., 2011. Stimulation of both photosynthesis and respiration in response to warmer and drier conditions in a boreal peatland ecosystem. Glob. Chang. Biol. 17, 2271–2287. https://doi.org/10.1111/j.1365-2486.2010.02378.x.

Fortuniak, K., Pawlak, W., Bednorz, L., Grygoruk, M., Siedlecki, M., Zieliński, M., 2017. Methane and carbon dioxide fluxes of a temperate mire in Central Europe. Agric. For. Meteorol. 232, 306–318. https://doi.org/10.1016/j.agrformet.2016.08.023.

Fortuniak, K., Pawlak, W., Siedlecki, M., Chambers, S., Bednorz, L., 2021. Temperate mire fluctuations from carbon sink to carbon source following changes in water table. Sci. Total Environ. 756, 144071.

Friedlingstein, P., O'Sullivan, M., Jones, M.W., Andrew, R.M., Gregor, L., Hauck, J., Le Quéré, C., Luijkx, I.T., Olsen, A., Peters, G.P., Peters, W., Pongratz, J., Schwingshackl, C., Sitch, S., Canadell, J.G., Ciais, P., Jackson, R.B., Alin, S.R., Alkama, R., Arneth, A., Arora, V.K., Bates, N.R., Becker, M., Zheng, B., 2022. Global Carbon Budget 2022. Earth Syst. Sci. Data 14 (4811–4900). https://doi.org/10.5194/essd-14-4811-2022.

Gedney, N., Cox, P.M., Huntingford, C., 2004. Climate feedback from wetland methane emissions. Geophys. Res. Lett. 31 (20).

Gedney, N., Huntingford, C., Comyn-Platt, E., Wiltshire, A., 2019. Significant feedbacks of wetland methane release on climate change and the causes of their uncertainty. Environ. Res. Lett. 14, 084027.

Gelman, A., Carlin, J., Stern, H., Dunson, D., Vehtari, A., Rubin, D., 2013. Bayesian Data Analysis, 3rd edn. Chapman and Hall/CRC.

Harper, A.B., Cox, P.M., Friedlingstein, P., Wiltshire, A.J., Jones, C.D., Sitch, S., Mercado, L.M., Groenendijk, M., Robertson, E., Kattge, J., Bönisch, G., Atkin, O.K., Bahn, M., Cornelissen, J., Niinemets, U., Onipchenko, V., Peñuelas, J., Poorter, L., Reich, P.B., Soudzilovskaia, N.A., Bodegom, P.V., 2016. Improved representation of plant functional types and physiology in the Joint UK Land Environment Simulator (JULES v4.2) using plant trait information. Geosci. Model Dev. 9, 2415–2440. https://doi.org/10.5194/gmd-9-2415-2016. https://www.geosci-model-dev.net/9/2415/2016/.

Houska, T., Kraft, P., Chamorro-Chavez, A., Breuer, L., 2015. SPOTting model parameters using a ready-made Python package. PLoS One 10 (12), e0145180. https://doi.org/10.1371/journal.pone.0145180.

Huang, Y.Y., Ciais, P., Luo, Y., Zhu, D., Wang, Y., Qiu, C., Goll, D.S., Guenet, B., Makowski, D., De Graaf, I., Leifeld, J., Kwon, M.J., Hu, J., Qu, L., 2021. Tradeoff of CO_2 and CH_4 emissions from global peatlands under water-table drawdown. Nat. Clim. Chang. 11 (7), 618–622.

IPCC, 2021. Climate Change 2021: the physical science basis. In: Masson-Delmotte, V., Zhai, P., Pirani, A., Connors, S.L., Péan, C., Berger, S., Caud, N., Chen, Y., Goldfarb, L., Gomis, M.I., Huang, M., Leitzell, K., Lonnoy, E., Matthews, J.B.R.,

Maycock, T.K., Waterfield, T., Yelekçi, O., Yu, R., Zhou, B. (Eds.), Contribution of Working Group I to the Sixth Assessment Report of the Intergovernmental Panel on Climate Change. Cambridge University Press, Cambridge, United Kingdom and New York, NY, USA, p. 2391. https://doi.org/10.1017/9781009157896.

Joosten, H., 2009. The Global Peatland CO 2 Picture. Peatland Status and Drainage Related Emissions in All Countries of the World. Wetlands International. https://unfccc.int/files/kyoto_protocol/application/pdf/draftpeatlandco2report.pdf.

Kaiser, S., Göckede, M., Castro-Morales, K., Knoblauch, C., Ekici, A., Kleinen, T., Zubrzycki, S., Sachs, T., Wille, C., Beer, C., 2017. Process-based modelling of the methane balance in periglacial landscapes (JSBACH-methane). Geosci. Model Dev. 10, 333–358. https://doi.org/10.5194/gmd-10-333-2017.

Kleinen, T., Mikolajewicz, U., Brovkin, V., 2020. Terrestrial methane emission from the Last Glacial Maximum to the preindustrial period. Clim. Past 16 (2), 575–595.

Knox, S., Jackson, R.B., Poulter, B., McNicol, G., Fluet-Chouinard, E., Zhnag, Z., Hugelius, G., Bousuqet, P., Canadell, J.G., Saunois, M., Papale, D., Chu, H., Keenan, T., Baldocchi, D., Tom, M.S., Trotta, C., Mammarella, I., Aurela, M., Bohrer, G., Campbell, D., Cescatti, A., Chamberlain, S., Chen, J., Chen, W., Dengel, S., Desai, A.R., Euskirchen, E., Friborg, T., Gasbarra, D., Goded, I., Goeckede, M., Heimann, M., Helbig, M., Hirano, T., Hollinger, D.Y., Iwata, H., Kang, M., Klatt, J., Kraus, K.W., Kutzbach, L., Lohila, A., Mitra, B., Morin, T.H., Nilsson, M.B., Niu, S., Noomets, A., Oechel, W.C., Peichl, M., Peltola, O., Reba, M.L., Runkle, B.R.K., Richardson, A.D., Ryu, Y., Sachs, T., Shcäfer, K.V.R., Scmid, H.P., Shurpali, N., Sonnentag, O., Tang, A.C.I., Ueyama, M., Vargas, R., Vesala, T., Ward, E.J., Windham-Myers, L., Wohlfahrt, G., Zona, D., 2019. FLUXNET-CH_4 synthesis activity: objectives, observations, and future directions. Bull. Am. Meteorol. Soc. 100 (12), 2607–2632.

Korrensalo, A., Mammarella, I., Alekseychik, P., Vesala, T., Tuittila, E.S., 2022. Plant mediated methane efflux from a boreal peatland complex. Plant Soil 1-18.

Lafleur, P.M., Roulet, N.T., Bubier, J.L., Frolking, S., Moore, T.R., 2003. Interannual variability in the peatland-atmosphere carbon dioxide exchange at an ombrotrophic bog. Glob. Biogeochem. Cycles 17 (2), 1036. https://doi.org/10.1029/2002GB001983.

Lafleur, P.M., Moore, T.R., Roulet, N.T., Frolking, S., 2005. Ecosystem respiration in a cool temperate bog depends on peat temperature but not water table. Ecosystems 8, 619–629. https://doi.org/10.1007/s10021-003-0131-2.

Laine, A.M., Korrensalo, A., Tuittila, E.S., 2022. Plant functional traits play the second fiddle to plant functional types in explaining peatland CO_2 and CH_4 gas exchange. Sci. Total Environ. 834, 155352.

Lehner, B., Döll, P., 2004. Development and validation of a global database of lakes, reservoirs and wetlands. J. Hydrol. 296, 1–22. https://doi.org/10.1016/j.jhydrol.2004.03.028.

Li, X., Markkanen, T., Korkiakoski, M., Lohila, A., Leppänen, A., Aalto, T., Peltoniemi, M., Mäkipää, R., Kleinen, T., Raivonen, M., 2024. Modelling alternative harvest effects on soil CO_2 and CH_4 fluxes from peatland forests. Sci. Total Environ. 951, 175257. https://doi.org/10.1016/j.scitotenv.2024.175257.

Lohila, A., Aurela, M., Hatakka, J., Pihlatie, M., Minkkinen, K., Penttilä, T., Laurila, T., 2010. Responses of N2O fluxes to temperature, water table and N deposition in a northern boreal fen. Eur. J. Soil Sci. 61 (5), 651–661.

Long, K.D., Flanagan, L.B., Cai, T., 2010. Diurnal and seasonal variation in methane emissions in a northern Canadian peatland measured by eddy covariance. Glob. Chang. Biol. 16, 2420–2435. https://doi.org/10.1111/j.1365-2486.2009.02083.x.

Lupascu, M., Wadham, J.L., Hornibrook, E.R., Pancost, R.D., 2012. Temperature sensitivity of methane production in the permafrost active layer at Stordalen, Sweden: a comparison with non-permafrost northern wetlands. Arct. Antarct. Alp. Res. 44 (4), 469–482.

Mastepanov, M., Sigsgaard, C., Tagesson, T., Ström, L., Tamstorf, M.P., Lund, M., Christensen, T.R., 2013. Revisiting factors controlling methane emissions from high-Arctic tundra. Biogeosciences 10, 5139–5158. https://doi.org/10.5194/bg-10-5139-2013.

Melton, J.R., Wania, R., Hodson, E.L., Poulter, B., Ringeval, B., Spahni, R., Bohn, T., Avis, C.A., Beerling, D.J., Chen, G., Elissev, A.V., Denisov, S.N., Hopcroft, P.O., Lettenmaier, D.P., Riley, W.J., Singarayer, J.S., Subin, Z.M., Tian, H., Zürcher, S., Brovkin, V., van Bodegom, P.M., Kleinen, T., Yu, Z.C., Kaplan, J.O., 2013. Present state of global wetland extent and wetland methane modelling: conclusions from a model inter-comparison project (WETCHIMP). Biogeosciences 10 (2), 753–788.

Moore, T.R., Bubier, J.L., Frolking, S.E., Lafleur, P.M., Roulet, N.T., 2002. Plant biomass and production and CO_2 exchange in an ombrotrophic bog. J. Ecol. 90, 25–36.

Moore, T.R., De Young, A., Bubier, J.L., Humphreys, E.R., Lafleur, P.M., Roulet, N.T., 2011. A multi-year record of methane flux at the Mer Bleue bog, southern Canada. Ecosystems 14 (4), 646–657.

Myhre, G., Shindell, D., Bréon, F.-M., Collins, W., Fuglestvedt, J., Huang, J., Koch, D., Lamarque, J.-F., Lee, D., Mendoza, B., Nakajima, T., Robock, A., Stephens, G., Takemura, T., Zhang, H., 2013. Anthropogenic and natural radiative forcing. In: Stocker, T.F., Qin, D., Plattner, G.-K., Tignor, M., Allen, S.K., Doschung, J., Nauels, A., Xia, Y., Bex, V., Midgley, P.M. (Eds.), Climate Change 2013: The Physical Science Basis. Contribution of Working Group I to the Fifth Assessment Report of the Intergovernmental Panel on Climate Change. Cambridge University Press, pp. 659–740. https://doi.org/10.1017/CBO9781107415324.018.

Nedwell, D.B., Watson, A., 1995. CH_4 production, oxidation and emission in a U.K. ombrotrophic peat bog: influence of SO_2^{-4} from acid rain. Soil Biol. Biochem. 27, 893–903. https://doi.org/10.1016/0038-0717(95)00018-A.

Nevalainen, O., 2022. Ollinevalainen/satellitetools: v1.0.0 (v1.0.0). Zenodo. https://doi.org/10.5281/zenodo.5993292.

Nilsson, M., Sagerfors, J., Buffam, I., Laudon, H., Eriksson, T., Grelle, A., Klemedtsson, L., Weslien, P., Lindroth, A., 2008. Contemporary carbon accumulation in a boreal oligotrophic minerogenic mire–a significant sink after accounting for all C-fluxes. Glob. Chang. Biol. 14 (10), 2317–2332.

Peltola, O., Vesala, T., Gao, Y., Räty, O., Alekseychik, P., Aurela, M., Chojnicki, B., Desai, A.R., Dolman, A.J., Euskirchen, E.S., Friborg, T., Göckede, M., Helbig, M., Humphreys, E., Jackson, R.B., Jocher, G., Joos, F., Klatt, J., Knox, S.H., Kowalska, N., Kutzbach, L., Lienert, S., Lohila, A., Mammarella, I., Nadeau, D.F., Nilsson, M.B., Oechel, W.C., Peichl, M., Pypker, T., Quinton, W., Rinne, J., Sachs, T., Samson, M., Schmid, H.P., Sonnentag, O., Wille, C., Zona, D., Aalto, T., 2019. Monthly gridded data product of northern wetland methane emissions based on upscaling eddy covariance observations. Earth System Science Data 11 (3), 1263–1289.

Pirinen, P., Simola, H., Aalto, J., Kaukoranta, J.P., Karlsson, P., Ruuhela, R., 2012. Tilastoja Suomen ilmastosta 1981–2010, [Climatological statistics of Finland 1981–2010.], Finnish Meteorological Institute, Reports 1/2012, Helsinki, 83 pp. Finnish with English Summary.

Qiu, C., Zhu, D., Ciais, P., Guenet, B., Peng, S., Krinner, G., Tootchi, A., Ducharne, A., Hastie, A., 2019. Modelling northern peatland area and carbon dynamics since the Holocene with the ORCHIDEE-PEAT land surface model (SVN r5488). Geosci. Model Dev. 12 (7), 2961–2982.

Qiu, C., Ciais, P., Zhu, D., Guenet, B., Chang, J., Chaudhary, N., Kleinen, T., Li, X.Y., Westermann, S., 2022. A strong mitigation scenario maintains climate neutrality of northern peatlands. One Earth 5 (1), 86–97.

Raivonen, M., Smolander, S., Backman, L., Susiluoto, J., Aalto, T., Markkanen, T., Mäkelä, J., Rinne, J., Peltola, O., Aurela, M., Tomasic, M., Li, X.F., Larmola, T., Juutinen, S., Tuittila, E.-S., Heimann, M., Sevanto, S., Kleinen, T., Brovkin, V., Vesala, T., 2017. HIMMELI v1. 0: HelsinkI model of MEthane buiLd-up and emIssion for peatlands. Geosci. Model Dev. 10, 4665–4691.

Riley, W.J., Subin, Z.M., Lawrence, D.M., Swenson, S.C., Torn, M.S., Meng, L., Mahowald, N.M., Hess, P., 2011. Barriers to predicting changes in global terrestrial methane fluxes: analyses using CLM4Me, a methane biogeochemistry model integrated in CESM. Biogeosciences 8, 1925–1953. https://doi.org/10.5194/bg-8-1925-2011.

Rinne, J., Riutta, T., Pihlatie, M., Aurela, M., Haapanala, S., Tuovinen, J.-P., Tuittila, E.-S., Vesala, T., 2007. Annual cycle of methane emission from a boreal fen measured by the eddy covariance technique. Tellus Ser. B Chem. Phys. Meteorol. 59, 449–457. https://doi.org/10.1111/j.1600-0889.2007.00261.x.

Rinne, J., Tuittila, E.-S., Peltola, O., Li, X., Raivonen, M., Alekseychik, P., Haapanala, S., Pihlatie, M., Aurela, M., Mammarella, I., Vesala, T., 2018. Temporal variation of ecosystem scale methane emission from a boreal fen in relation to temperature, water table position, and carbon dioxide fluxes. Global Biogeochem. Cy. 32, 1087–1106. https://doi.org/10.1029/2017GB005747.

Rosentreter, J.A., Borges, A.V., Deemer, B.R., Holgerson, M.A., Liu, S., Song, C., Melack, J., Raymond, P.A., Duarte, C.M., Allen, G.H., Olefeldt, D., Poulter, B., Battin, T.I., Eyre, B.D., 2021. Half of global methane emissions come from highly variable aquatic ecosystem sources. Nat. Geosci. 14 (4), 225–230.

Rosenzweig, C., Arnell, N.W., Ebi, K.L., Lotze-Campen, H., Raes, F., Rapley, C., Smith, M. S., Cramer, W., Frieler, K., Reyer, C.P., Schewe, J., van Vuuren, D., Warszawski, L., 2017. Assessing inter-sectoral climate change risks: the role of ISIMIP. Environ. Res. Lett. 12, 010301.

Roulet, N.T., Lafleur, P.M., Richard, P.J., Moore, T.R., Humphreys, E.R., Bubier, J., 2007. Contemporary carbon balance and late holocene carbon accumulation in a northern peatland. Glob. Chang. Biol. 13, 397–411.

Sagerfors, J., Lindroth, A., Grelle, A., Klemedtsson, L., Weslien, P., Nilsson, M.B., 2008. Annual CO_2 exchange between a nutrient-poor, minerotrophic, boreal mire and the atmosphere. J. Geophys. Res.-Biogeo. 113, 1–15. https://doi.org/10.1029/2006JG000306.

Salmon, E., Jégou, F., Guenet, B., Jourdain, L., Qiu, C., Bastrikov, V., Guimbaud, C., Zhu, D., Ciais, P., Peylin, P., Gogo, S., Laggoun-Défarge, F., Aurela, M., Bret-Harte, M.S., Chen, J., Chojnicki, B.H., Chu, H., Edgar, C.W., Euskirchen, E.S., Flanagan, L.B., Fortuniak, K., Holl, D., Klatt, J., Kolle, O., Kowalska, N., Kutzbach, L., Lohila, A., Merbold, L., Pawlak, W., Sachs, T., Ziemblińska, K., 2022. Assessing methane emissions for northern peatlands in ORCHIDEE-PEAT revision 7020. Geosci. Model Dev. 15 (7), 2813–2838.

Saunois, M., Martinez, A., Poulter, B., Zhang, Z., Raymond, P., Regnier, P., Canadell, J.G., Jackson, R.B., Patra, P.K., Bousquet, P., Ciais, P., Dlugokencky, E.J., Lan, X., Allen, G.H., Bastviken, D., Beerling, D.J., Belikov, D.A., Blake, D.R., Castaldi, S., Crippa, M., Deemer, B.R., Dennison, F., Etiope, G., Gedney, N., Höglund-Isaksson, L., Holgerson, M.A., Hopcroft, P.O., Hugelius, G., Ito, A., Jain, A.K., Janardanan, R., Johnson, M.S., Kleinen, T., Krummel, P., Lauerwald, R., Li, T., Liu, X., McDonald, K. C., Melton, J.R., Mühle, J., Müller, J., Murguia-Flores, F., Niwa, Y., Noce, S., Pan, S., Parker, R.J., Peng, C., Ramonet, M., Riley, W.J., Rocher-Ros, G., Rosentreter, J.A., Sasakawa, M., Segers, A., Smith, S.J., Stanley, E.H., Thanwerdas, J., Tian, H., Tsuruta, A., Tubiello, F.N., Weber, T.S., van der Werf, G., Worthy, D.E., Xi, Y., Yoshida, Y., Zhang, W., Zheng, B., Zhu, Q., Zhu, Q., Zhuang, Q., 2024. Global Methane Budget 2000–2020. Earth Syst. Sci. Data Discuss. https://doi.org/10.5194/essd-2024-115 [preprint]. in review.

Segers, R., 1998. Methane production and methane consumption: a review of processes underlying wetland methane fluxes. Biogeochemistry 41, 23–51.

Sellar, A.A., Jones, C.G., Mulcahy, J., Tang, Y., Yool, A., Wiltshire, A., O'connor, F.M., Stringer, M., Hill, R., Palmieri, J., Zerroukat, M., 2019. UKESM1: description and evaluation of the UK earth system model. Journal of Advances in Modeling Earth Systems 11, 4513–4558.

Smith, K.A., Ball, T., Conen, F., Dobbie, K.E., Massheder, J., Rey, A., 2003. Exchange of greenhouse gases between soil and atmosphere:interactions of soil physical factors and biological processes. Eur. J. Soil Sci. 54, 779–791.

Smith, N.D., Burke, E.J., Schanke Aas, K., Althuizen, I.H.J., Boike, J., Christiansen, C.T., Etzelmüller, B., Friborg, T., Lee, H., Rumbold, H., Turton, R.H., Westermann, S.,

Chadburn, S.E., 2022. Explicitly modelling microtopography in permafrost landscapes in a land surface model (JULES vn5.4_microtopography). Geosci. Model Dev. 15 (9), 3603–3639.
Sriskantharajah, S., Fisher, R.E., Lowry, D., Aalto, T., Hatakka, J., Aurela, M., Laurila, T., Lohila, A., Kuitunen, E., Nisbet, E.G., 2012. Stable carbon isotope signatures of methane from a Finnish subarctic wetland. Tellus B 64, 18818. https://doi.org/10.3402/tellusb.v64i0.18818.
Stephen, K., Arah, J., Thomas, K., Benstead, J., Lloyd, D., 1998. Gas diffusion coefficient profile in peat determined by modelling mass spectrometric data: implications for gas phase distribution. Soil Biol. Biochem. 30, 429–431. https://doi.org/10.1016/S0038-0717(97)00118-1.
Sun, X., Song, C., Guo, Y., Wang, X., Yang, G., Li, Y., Mao, R., Lu, Y., 2012. Effect of plants on methane emissions from a temperate marsh in different seasons. Atmos. Environ. 60, 277–282.
Susiluoto, J., Raivonen, M., Backman, L., Laine, M., Makela, J., Peltola, O., Vesala, T., Aalto, T., 2018. Calibrating the sqHIMMELI v1.0 wetland methane emission model with hierarchical modeling and adaptive MCMC. Geosci. Model Dev. 11 (3), 1199–1228.
Syed, K.H., Flanagan, L.B., Carlson, P.J., Glenn, A.J., Van Gaalen, K.E., 2006. Environmental control of net ecosystem CO2 exchange in a treed, moderately rich fen in northern Alberta. Agric. For. Meteorol. 140 (1-4), 97–114.
Turetsky, M.R., Kotowska, A., Bubier, J., Dise, N.B., Crill, P., Hornibrook, E.R., Minkkinen, K., Moore, T.R., Myers-Smith, I.H., Nykänen, H., Olefeldt, D., Rinne, J., Saarnio, S., Shurpali, N., Tuittila, E.-S., Waddington, J.M., White, J.R., Wickland, K. P., Wilmking, M., 2014. A synthesis of methane emissions from 71 northern, temperate, and subtropical wetlands. Glob. Chang. Biol. https://doi.org/10.1111/gcb.12580.
Tyystjärvi, V., Markkanen, T., Backman, L., Raivonen, M., Leppänen, A., Li, X., Ojanen, P., Minkkinen, K., Hautala, R., Peltoniemi, M., Anttila, J., Laiho, R., Lohila, A., Mäkipää, R., Aalto, T., 2024. Future methane fluxes of peatlands are controlled by management practices and fluctuations in hydrological conditions due to climatic variability. Biogeosciences 21, 5745–5771. https://doi.org/10.5194/bg-21-5745-2024.
van Huissteden, J., Petrescu, A.M.R., Hendriks, D.M.D., Rebel, K.T., 2009. Sensitivity analysis of a wetland methane emission model based on temperate and arctic wetland sites. Biogeosciences 6, 3035–3051. https://doi.org/10.5194/bg-6-3035-2009.
Wania, R., Ross, I., Prentice, I.C., 2010. Implementation and evaluation of a new methane model within a dynamic global vegetation model: LPJ-WHyMe v1.3.1. Geosci. Model Dev. 3, 565–584. https://doi.org/10.5194/gmd-3-565-2010.
Watson, A., Stephen, K.D., Nedwell, D.B., Arah, J.R.M., 1997. Oxidation of methane in peat: kinetics of CH_4 and O_2 removal and the role of plant roots. Soil Biol. Biochem. 29, 1257–1267.
Weedon, G.P., Gomes, S., Viterbo, P., Österle, H., Adam, J.C., Bellouin, N., Boucher, O., Best, M., 2010. The WATCH Forcing Data 1958–2001: A Meteorological Forcing Dataset for Land Surface-and Hydrological-Models. WATCH technical report.
Weedon, G.P., Balsamo, G., Bellouin, N., Gomes, S., Best, M.J., Viterbo, P., 2014. The WFDEI meteorological forcing data set: WATCH Forcing Data methodology applied to ERA-Interim reanalysis data. Water Resour. Res. 50 (9), 7505–7514.
Weiss, M., Baret, F., 2016. S2ToolBox Level 2 Products: LAI, FAPAR, FCOVER. available at: https://step.esa.int/docs/extra/ATBD_S2ToolBox_L2B_V1.1.pdf.
Wiltshire, A.J., Burke, E.J., Chadburn, S.E., Jones, C.D., Cox, P.M., Davies-Barnard, T., Friedlingstein, P., Harper, A.B., Liddicoat, S., Sitch, S., Zaehle, S., 2021. JULES-CN: a coupled terrestrial carbon–nitrogen scheme (JULES vn5.1). Geosci. Model Dev. 14, 2161–2186. https://doi.org/10.5194/gmd-14-2161-2021. https://gmd.copernicus.org/articles/14/2161/2021/.
Xu, X., Yuan, F., Hanson, P.J., Wullschleger, S.D., Thornton, P.E., Riley, W.J., Song, X., Graham, D.E., Song, C., Tian, H., 2016. Reviews and syntheses: four decades of modeling methane cycling in terrestrial ecosystems. Biogeosciences 13 (12), 3735–3755.
Xu, J., Morris, P.J., Liu, J., Holden, J., 2018. PEATMAP: refining estimates of global peatland distribution based on a meta-analysis. Catena 160, 134–140. https://doi.org/10.1016/j.catena.2017.09.010.
Yuan, K., Li, F., McNicol, G., Chen, M., Hoyt, A., Knox, S., Riley, W.J., Jackson, R., Zhu, Q., 2024. Boreal–Arctic wetland methane emissions modulated by warming and vegetation activity. Nat. Clim. Chang. 14, 282–288. https://doi.org/10.1038/s41558-024-01933-3.
Yvon-Durocher, G., Allen, A.P., Bastviken, D., Conrad, R., Gudasz, C., St-Pierre, A., Thanh-Duc, N., Del Giorgio, P.A., 2014. Methane fluxes show consistent temperature dependence across microbial to ecosystem scales. Nature 507 (7493), 488.
Zhang, Z., Fluet-Chouinard, E., Jensen, K., McDonald, K., Hugelius, G., Gumbricht, T., Carroll, M., Prigent, C., Bartsch, A., Poulter, B., 2021. Development of the global dataset of wetland area and dynamics for methane modeling (WAD2M). Earth System Science Data 13 (5), 2001–2023.
Zhang, H., Tuittila, E.-S., Korrensalo, A., Laine, A.M., Uljas, S., Welti, N., Kerttula, J., Maljanen, M., Elliott, D., Vesala, T., Lohila, A., 2021. Methane production and oxidation potentials along a fen-bog gradient from southern boreal to subarctic peatlands in Finland. Glob. Chang. Biol. 27 (18), 4449–4464.
Zhang, Z., Poulter, B., Feldman, A.F., Ying, Q., Ciais, P., Peng, S., Li, X., 2023. Recent intensification of wetland methane feedback. Nat. Clim. Chang. 13, 430–433. https://doi.org/10.1038/s41558-023-01629-0.
Zhuang, Q., Melillo, J.M., Kicklighter, D.W., Prinn, R.G., McGuire, A.D., Steudler, P.A., Felzer, B.S., Hu, S., 2004. Methane fluxes between terrestrial ecosystems and the atmosphere at northern high latitudes during the past century: a retrospective analysis with a process-based biogeochemistry model. Global Biogeochem. Cy. 18 (18), GB3010. https://doi.org/10.1029/2004GB002239.